Theoretical and experimental contributions to the understanding of foam drainage

Peters, E.A.J.F.

Award date:
1995

Eindhoven University of Technology
Department of Applied Physics
Theoretical Physics

Theoretical and Experimental Contributions to the Understanding of Foam Drainage

E.A.J.F. Peters

August 1995

Master thesis

Study performed at the department Engeneering Physics of the Koninklijke/Shell-Laboratorium, Amsterdam

Advisor: Dr. G. Verbist
Supervisor: Prof. Dr. M.A.J. Michels

Committee: Dr. A. Hirschberg
Prof. Dr. W. de Jonge
Dr. L. Kamp
Prof. Dr. M. Michels
Dr. G. Verbist

Abstract

Drainage of liquid in polyhedral foams (i.e. dry foams) is studied, both theoretically and experimentally. The foam is a structure of films and of channels that are formed where the films meet. Most of the liquid is contained in these channels called Plateau borders. The Plateau borders form a network. A theory has been developed that describes drainage through a dry foam as governed by Poiseuille flow through Plateau borders.

Effective material properties are derived for these Plateau border networks. To include contributions of the films and of the gas phase (in the case of, e.g; permittivity) we used a preliminary effective medium theory.

To describe the drainage of liquid through the foam, the Poiseuille flow driven by gravity and Laplace-pressure differences (caused by the surface tension), are combined with the network theory. A nonlinear model with solitary-wave solutions is discussed.

Forced and free drainage through a foam are studied experimentally. As new methods segmented capacitance and conductance measurements are introduced. We used a column (2cm width, 70cm high) with an aqueous foam which was wetted from above.

Most measurements were done with a capacitance *level gauge*. During this traineeship a new conductance level gauge with better characteristics was developed.

Measurements were used to verify the theory. Solitary waves were measured and we found quantitative results supporting the theory. Besides solitary waves, free drainage profiles and propagating pulses were studied. When studying double waves some yet unexplained phenomena were observed.

To complete the circle we used the effective-medium theory for the calibration curves of the level gauges.

Preface

First of all I would like to thank Guy Verbist for his excellent and inspiring advises, both concerning this project but also concerning private matters.

Without the experimental genius of Hans van der Steen, this project would not have been possible. I would like to thank him for devoting so much of his time to it. Thanks are due to N. van Oss for selecting the right surfactant.

Although I never met him, my predecessor S. Hutzler was very helpful. His work was an excellent basis for me to start from. I would like to thank D. Weaire for his invaluable theoretical support.

I am grateful for Thijs Michels, Guy and most of the other members of the department Engineering Physics for helping me find a PhD. position. Furthermore I would like to thank everyone at E.P. and all the trainees I met for the wonderful time they gave me here in Amsterdam,

Frank Peters.

Contents

Chapter 1

Introduction

The traineeship for this final project was done at the Royal/Shell Laboratory Amsterdam in the department Engineering Physics. The topic was foam drainage.

Foams are quasi stationary structures with an enhanced gas-liquid interface. In the study presented here we are especially interested in dry foams (less than 20 % liquid). These foams have a special structure: where two bubbles meet films are formed, where three bubbles meet channels (called Plateau borders) are formed. The foam will try to minimise the total area of its internal gas-liquid interfaces. It is however limited to destroy the internal structures because of particular stabilising effects in these structures (i.e. in films and Plateau borders). The result is the typical foam structure where almost all liquid is contained in the Plateau borders. The films are *sucked* empty by the Plateau borders. The same effect can be seen for a soap film in a wire frame. Here too the film is sucked empty and becomes so thin that even optical interference effects are observed.

For a company like Shell knowledge of foams is invaluable. Foam is an annoying factor in many chemical processes. In a distillation column foam might cause a thermal bridge between trays in the column. This will decrease the efficiency of the separation process terribly. The chemical industry wants to control foaming. If they cannot control it they have to incorporate it phenomenologically when designing a chemical plant. This means overdimensionalising and thus extra inefficiencies and costs. The way people try to predict foamability is by doing foam tests. In a column with a certain amount of liquid, gas is introduced and the height of the formed foam is measured as function of the gas rate. In practice the foamability under laboratory conditions does not always relate to the foam formation under reactor conditions. Foam is still very unpredictable and theories characterising foams are therefore needed badly in the industry.

Industry does not only want to study foam to reduce its occurence in processes, they commercially produce foams as well. Many foams are produced in the food industry (e.g; bread, deserts). But a company like Shell produces them too. They blow for example polyurethane foam (used in car seats and for isolation purposes). Because of environmental legislations existing processes have to be modified to avoid the use of CFCs. This means that phenomenological knowledge, has to be replaced by new knowledge in the short term in order to keep up the product

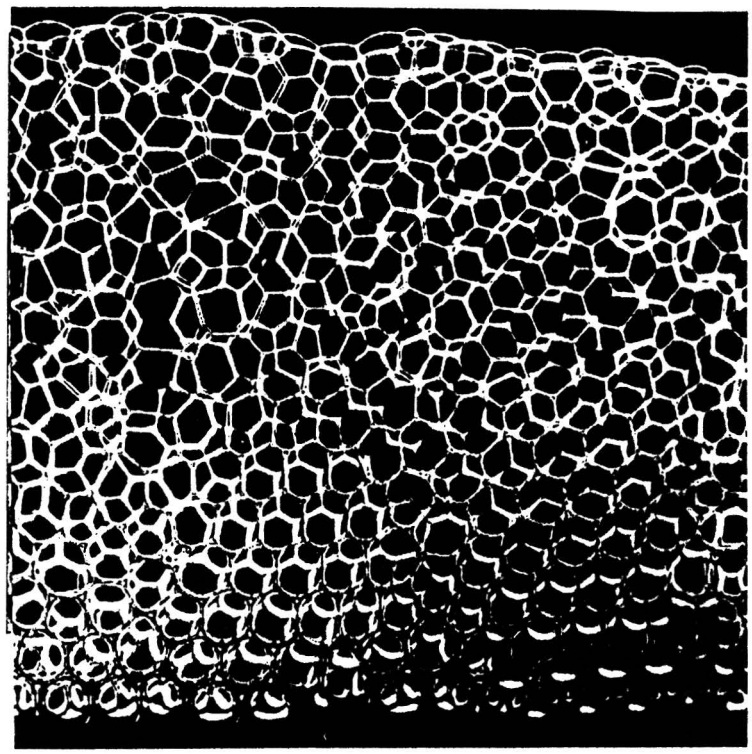

Figure 1.1: *A dry foam. Almost all liquid is in the Plateau borders. That is why it is so transparent.*

quality. The basic question is how to control the properties of the resulting end product. Matters of concern include the structure of the produced foam, e.g; will it have an open or closed structure?

At Shell much research is done on interfacial stability in relation to thin films as they exist in foams. Most of this is research at the molecular level. Major topics are: what determines soap film stability and what are the mechanisms of micelle formation. Theoretical techniques used in this research are mostly computer simulations using Brownian dynamics or molecular dynamics.

The topic of this report concerns more macroscopic aspects of foam. We describe the foam as a static, stable, non-changing structure with liquid flowing through it. Until recently this was an underappreciated side in studies of foam stability.

Stability is the keyword for foams. A foam attains its characteristic properties from surface active molecules, surfactants. They lower the surface tension (otherwise they would not be surface active). A lower surface tension alone however does not provide stability. Surfactants give rise to other kinds of stabilising effects. An important one for soap films is the Marangoni effect. When soap surfaces are perturbed locally, there is a local expansion of the surface. Because the density of surfactants is higher at the surface than in the bulk, this means temporarily a decrease of surfactants per unit area. This decrease has as a consequence that the surface tension increases locally. So a rapid local increase of surface area gives a local increase of surface tension and therefore an extra stabilising effect. When

films get thinner other effects take over. Molecular interactions of the surfactants at opposing surfaces of the film give stabilising effects. All these phenomena have characteristic time scales, for example depending on the diffusion rate of the surfactants to the film surface.

The *lifetime* of a foam is related to the stabilising effects. Soap films will drain into the Plateau borders where the films meet. Depending on the thickness of the films, they will be in a different stability regime. In all these regimes the films will have a specific life time after which it snaps and structural changes happen in the foam. The drainage of liquid out of the films will be related to the pressure in the Plateau borders. This makes Plateau borders very significant for foam stability.

For dry foam (less than 20% liquid) most of the liquid will be in the Plateau borders. In this report we will study the drainage of liquid through such a foam. We describe solitary wave behaviour which is very easily verified experimentally. Furthermore the simple model, which is discussed, allows for quantitative verification using segmented probes developed and calibrated in the course of the work presented.

The presented theory can contribute to the theoretical insight in the foamability of substances, the theory can possibly make good predictions on how the liquid distributions will be in different production methods of, e.g; polyurethane foams. It can enhance knowledge of the product properties foams.

Besides describing the drainage of foams, we also describe an effective medium theory of a dry foam. We will use it here to describe electrical properties like conductance and capacitance. It might also be used to describe thermal conductance in a foam which relates to the thermal isolation properties.

This introduction was meant to give some more insight in the motivation for a company like Shell to do this kind of research. The other point I wanted to make, was the place of this theory between other foam theories. We will now proceed and present the most significant results of this traineeship at Shell. First some hard core theory, then some pleasant experimental data with pleasing graphs, have fun!

Chapter 2

Flow in a Plateau border

A Plateau border is the channel that is formed where three bubbles meet. The film between two bubbles contains virtually no liquid. A mechanism called marginal regeneration, driven by the higher Laplace pressure in the film (less curvature), thins the film by a combination of suction and stretching. This drainage of the soap film stops when interaction of surfactants at the opposite surfaces of the film prevent further thinning.

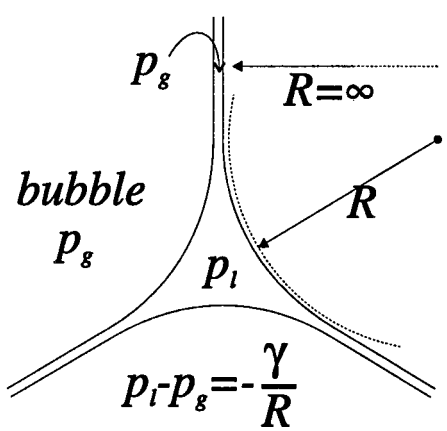

Figure 2.1: *Relation between pressure and wall curvature in a Plateau border.*

The pressure difference between a Plateau Border and the gas in the bubble is given by

$$p_g - p_l = \Delta p = \gamma \left(R_1^{-1} + R_2^{-1}\right), \tag{2.1}$$

where R_1 and R_2 are the principal radii of curvature (see A for a derivation). Roughly speaking the three sides of a Plateau border are cylindrical surfaces and hence $R_2 = \infty$. If we assume the pressure in all the bubbles is equal, say approximately atmospheric, the area of a Plateau border ($\mathcal{A}$) and the pressure (p_l) are

$$\begin{aligned} \mathcal{A} &= C_{area} R^2 \\ p_l &= p_g - \tfrac{\gamma}{R}, \end{aligned} \tag{2.2}$$

where $R = R_1$ is the remaining radius of curvature and C_{area} a numerical constant which will be derived below.

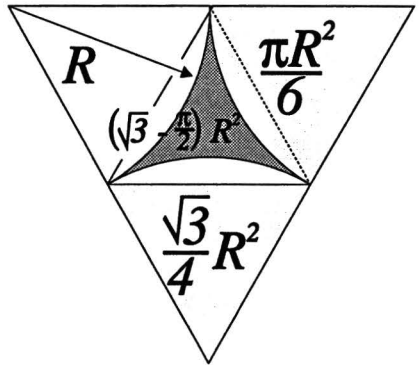

Figure 2.2: *The area of a Plateau border.*

The computation of C_{area} is elementary geometry, the sort the ancient Greeks enjoyed doing. It is illustrated in Fig. 2.2, and results in $C_{area} = \sqrt{3}-\pi/2 \approx 0.161$. If we look upon the Plateau border as a tube, this gives the restriction

$$\frac{\partial R}{\partial z} \ll 1 \tag{2.3}$$

If we make a second assumption that the surface viscosity is large enough to apply a no-slip boundary condition at the wall, then the flow through the Plateau border can be treated as Poiseuille flow. Poiseuille flow in the xy-plane with a constant pressure gradient in the z-direction obeys

$$\left(\frac{\partial^2}{\partial x^2}+\frac{\partial^2}{\partial y^2}\right) v(x,y) = \frac{1}{\eta}\frac{\partial p}{\partial z}, \qquad (x,y) \in A, \tag{2.4}$$

where η is the liquid viscosity, p the pressure. A is the cross sectional region of the pipe. For points on the boundary ∂A, the no-slip boundary condition translates to

$$v(x,y) = 0, \qquad (x,y) \in \partial A. \tag{2.5}$$

On dimensional grounds we expect the mean velocity u to be given by

$$\begin{aligned} u = \langle v \rangle = \frac{1}{\mathcal{A}} \int v(x,y)\, dxdy &= -\frac{1}{C_{\text{disp}}\,\eta}\frac{\partial p}{\partial z}\mathcal{A} \\ &= -\frac{1}{\eta^*}\frac{\partial p}{\partial z}\mathcal{A} \end{aligned} \tag{2.6}$$

where $\mathcal{A}$ is the area of A and C_{disp} a constant only dependent on the shape of the cross section of the tube. We call η^* the effective viscosity for that specific shape. This constant will be computed here for a Plateau border by numerically solving

$$\begin{aligned} \Delta v(x,y) &= -1, & v(x,y) \in A, \\ v(x,y) &= 0, & v(x,y) \in \partial A, \end{aligned} \tag{2.7}$$

where the boundary is defined as

$$\partial A: \; r(\phi) = \frac{2}{\sqrt{3}}\left[\cos\left(\phi \bmod \frac{2\pi}{3} - \frac{\pi}{3}\right) - \sqrt{\cos\left(\phi \bmod \frac{2\pi}{3} - \frac{\pi}{3}\right)^2 - 1/4}\right]. \tag{2.8}$$

area	C_{disp} (analytical)	C_{disp} (numerical)
circle	$8\pi = 25.13274$	25.13284
triangle	$20\sqrt{3} = 34.64102$	34.64088
Plateau border	-	49.69930

Table 2.1: C_{disp} *as computed for three shapes.*

First we note that $v_p(x, y) = -\frac{1}{4}r^2$ is a particular solution of Eq. (2.7). Therefore the homogeneous solution $v_h \equiv v - v_p$ must satisfy $\Delta v_h = 0$, with boundary condition $v_h(\partial A) = -v_p(\partial A)$. These last equations were solved using a numerical scheme that used a boundary integral method for solving the Laplace equation. To get an idea of the precision of the numerical code we obtained the constant C_{disp} as it occurs in solving Poiseuille flow for three different shapes namely a circle, a triangle and a Plateau border. For a circle and a triangle exact results are known and shown in Tab. 2.1 together with the computed results.

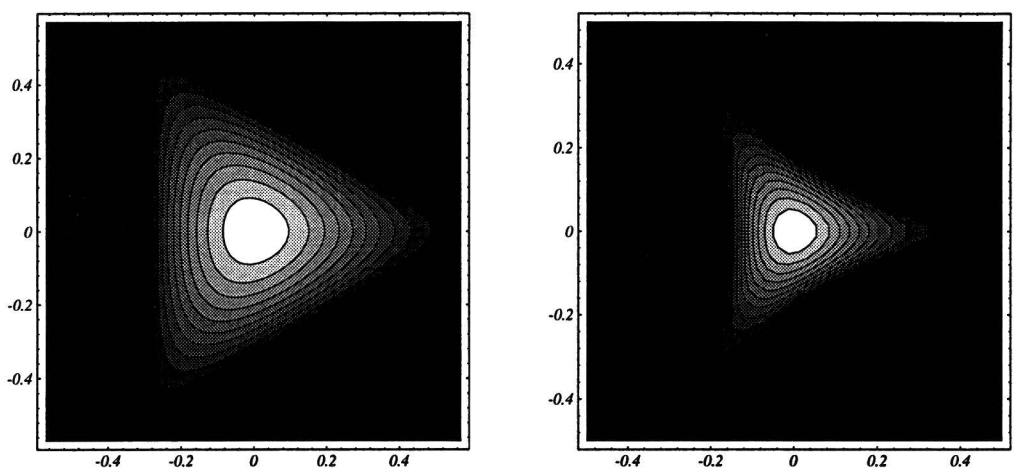

Figure 2.3: *Velocity profile $v(x, y)$, for a triangular area and for a Plateau border.*

In figure Fig. 2.3 the contour plots for a triangular area and for a Plateau border are given. The corner points for both are are $(0.58, 0)$,$(-0.29, 0.5)$,$(-0.29, -0.5)$. The flow in the corners of the Plateau border is very small. Using Tab. 2.1 we get that a Plateau border is equivalent to a triangle with has corner points which are a factor 0.83 its original distances apart. In this case that would mean that the corner points of this virtual triangle would be $(0.48, 0)$,$(-0.24, 0.42)$,$(-0.24, -0.42)$. Fig. 2.4 gives a three dimensional plot of the profile in a Plateau border. We always take the gas pressure in the bubbles to be equal so that we get nice symmetric Plateau borders. It is expected that if the Plateau borders are less symmetric the effective viscosity will be still larger.

In reality a network of Plateau borders, contains Plateau borders with many different orientations. This will be discussed in the next chapter (Ch. 3). The vertical orientation is a very special case. For a Plateau border in a gravitational field (directed along the z-axis), a pressure gradient in the z-direction and an

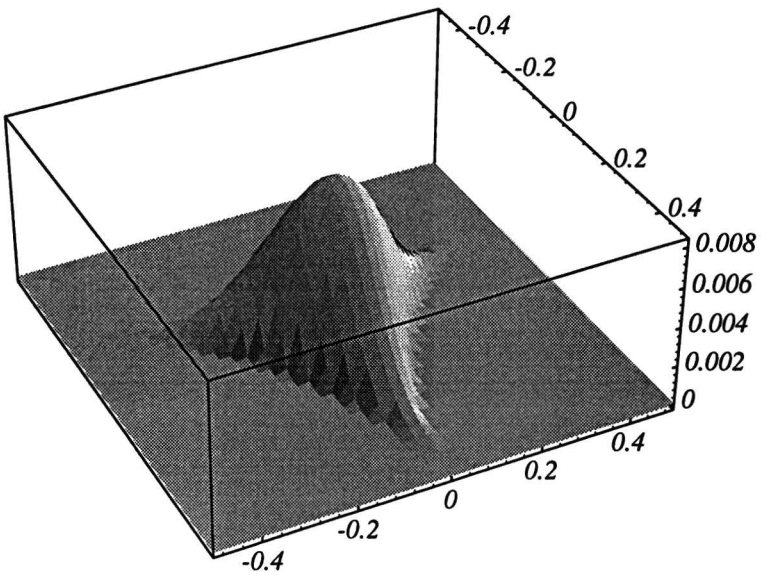

Figure 2.4: *Velocity profile $v(x, y)$, for a Plateau border.*

orientation θ_i as illustrated in Fig. 2.5, we find

$$\begin{aligned} u_i &= -\frac{1}{\eta^*}\mathcal{A}_i \, \nabla(p - \rho g z) \cdot \mathbf{e}_i \\ &= \frac{1}{\eta^*}\mathcal{A}_i \left(\rho g - \frac{\partial p}{\partial z}\right) \cos\theta_i. \end{aligned} \tag{2.9}$$

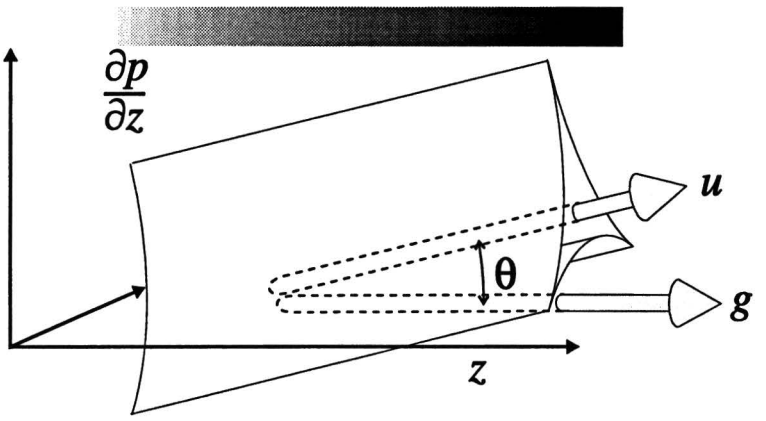

Figure 2.5: *Poiseuille flow through a Plateau border.*

In this report we try to describe drainage as flow through a network of Plateau borders. We have now one of the pillars this description rests upon, namely the flow through one Plateau border. This chapter had two main results. The first one was the relation between the pressure in a Plateau border and its area. The

second one was the computation of the effective viscosity of an ideally shaped Plateau border. This was very relevant because the effective viscosity and the viscosity appeared to differ more than one magnitude. In the next chapter (§3.2) will be shown how to take the network structure into account, this is the second pillar that supports the theory. The two pillars are put together in chapter 4, this will give an equation governing drainage. It is there we will also look to the properties of this equation and to its solutions.

Chapter 3

Effective material properties in a dry foam

In this chapter the foam is modeled as a network of Plateau borders and general expressions for overall effective properties in such a dry foam will be derived.

We will consider a foam in an external vector field. This field will be the gradient of some potential field ϕ e.g; a pressure field, or an electrical potential. The vector field induces a current density $\mathbf{j}$ proportional to the field, e.g; a liquid flow, an electric current or an electric displacement. The proportionality coefficient σ is some material property (e.g conductivity). The material property σ can be position dependent. Although the material constants inside the liquid and in the gas of the bubbles are known, our aim is to compute the effective constant for the foam.

To calculate such an effective property we assume steady state conditions, implying zero divergence for the current density. The governing equations become

$$\begin{aligned} \nabla \cdot \mathbf{j} &= 0 \\ \mathbf{j} &= -\sigma \nabla \phi. \end{aligned} \tag{3.1}$$

Below we use the example of an electric potential ϕ and conductance σ. The resulting expressions are more general and, e.g; applicable to the the thermal conductivity

We assume zero conductance of the second (gas)phase ($\sigma_g = 0$). Using this assumption, and keeping in mind the network structure of the Plateau borders, we apply the Kirchoff laws. A mean potential (V_j) can be associated with every nodal point (j) where Plateau borders meet. The current in a Plateau border is denoted by I_i. For every Plateau border (i), with length l_i and cross sectional area $\mathcal{A}_i$ connecting nodal points j_1 and j_2, the total current is given by

$$I_i = -\frac{\sigma_l \mathcal{A}_i}{l_i}(V_{j_1} - V_{j_2}). \tag{3.2}$$

We will now build a continuum theory for the discrete network, i.e., we assume that all relevant physical quantities vary only appreciably on length scales much

larger than the typical Plateau border length. Using this continuum approach, we can approximate Eq. (3.2) by

$$\begin{aligned} I_i &= \frac{\sigma_l \mathcal{A}_i}{l_i}(V_{j_1} - V_{j_2}) \\ &= -\sigma_l \mathcal{A}_i \nabla V \cdot \mathbf{e}_i, \end{aligned} \tag{3.3}$$

where $\mathbf{e}_i$ is the unity vector pointing from nodal point j_1 to j_2, e.i. parallel along the Plateau border, and ∇V the gradient of the continuum potential field V. Until now we used only one of the Kirchhof laws (namely that a potential can be associated with a each nodal point). It isn't at all clear that the introduction of a continuum field was justified. In a random network of wires, the second law of Kirchhof (the sum of the currents at a nodal point is zero), wouldn't be satisfied on the small length scale when using Eq. (3.3). Plateau borders, however, form very characteristic nodal points. They have to meet in a tetrahedral configuration because of minimisation of surface energy and all have approximately the same area $\mathcal{A}_i$. For every nodal point (j) the tetrahedral configuration of Plateau borders i implies

$$\sum \mathbf{e}_i = 0 \Rightarrow \sum I_i = 0. \tag{3.4}$$

This makes the continuum approach consistent with the Kirchhof laws, because also his second law is satisfied at the micro scale of the Plateau borders when using Eq. (3.3).

On length scales much greater than this micro scale, we now can introduce various continuum fields like $\mathcal{A}(\mathbf{x})$ and $\mathbf{J}(\mathbf{x})$. The first is the mean Plateau border area, averaged over a volume around $\mathbf{x}$. The second is a macroscopic current density. This is defined as the current through a orientated surface element. An expression for this quantity will be derived in the next section §3.1. The vector field $\mathbf{J}$ has to be divergence free, or is under the non-stationary conditions the current in a continuity equation.

To summarise: a potential field (ϕ) gives rise to mean potentials (V_j) given at the nodal points of the Plateau borders. We then introduced a function $V(z)$ which is equal to V_j in the nodal points and gives rise to a current in the Plateau borders via Eq. (3.3). While introducing $V(\mathbf{x})$ a macroscopic current density $\mathbf{J}(\mathbf{x})$ was introduced which satisfies the continuity equation.

3.1 Averaging

In the section above averages were taken over large numbers of Plateau borders and macroscopic fields were introduced, which varied only appreciably over length scales larger then the Plateau border lengths. It remains to obtain a useful expression for the macroscopic current density $\mathbf{J}$.

We now consider the foam as a random structure of Plateau borders. We then can introduce the number of Plateau borders per unit volume $N(\mathbf{x})$, leaving aside density distributions dependent on orientations. The liquid fraction $\Phi_\ell(\mathbf{x})$ is the number of Plateau borders times the average Plateau border volume, because we

assume that all liquid is contained in those. We take for this volume $\mathcal{A}(\mathbf{x})\, l(\mathbf{x})$. $l(\mathbf{x})$ is the mean Plateau border length,

$$\Phi_\ell(\mathbf{x}) = N(\mathbf{x})\, \mathcal{A}(\mathbf{x})\, l(\mathbf{x}). \tag{3.5}$$

To calculate the current density $\mathbf{J}(\mathbf{x})$ we need to know the mean number of Plateau borders with orientation $\mathbf{e}_i$ intersecting the surface element with orientation $\mathbf{e}_n$. Secondly we have to work out what current is associated with such a Plateau border. The last matter has already been addressed in Eq. (3.3).

The (unnormalised) number of Plateau borders which intersect a surface element $dA\,\mathbf{e}_n$, with orientation $\mathbf{e}_i$ is

$$N(\mathbf{x})\, l(\mathbf{x})\, |\mathbf{e}_n \cdot \mathbf{e}_i|\, dA, \tag{3.6}$$

when the lengths are uncorrelated to the orientations. This is certainly true for randomly orientated Plateau borders. To compute the total current density we use Eq. (3.3) multiplied by Eq. (3.6). For a Plateau border with orientation $\mathbf{e}_i$ we then find with the use of the introduced field $\mathcal{A}(\mathbf{x})$ instead of $\mathcal{A}_i$ and with using the definition of the current density

$$\forall \mathbf{e}_n \qquad (\mathbf{J}(\mathbf{x}) \cdot \mathbf{e}_n)\, dA = -\sigma_l\, \mathcal{A}(\mathbf{x})\, N(\mathbf{x})\, l(\mathbf{x})\, (\nabla V \cdot \mathbf{e}_i)\, (\mathbf{e}_n \cdot \mathbf{e}_i)\, dA \tag{3.7}$$

There is an ambiguity in the orientation of a Plateau border, it can either be $\mathbf{e}_i$ or $-\mathbf{e}_i$. To calculate the current density we should use the one for which $\mathbf{e}_n \cdot \mathbf{e}_i$ is positive. When averaging over the orientations of Plateau borders we find

$$\mathbf{J}(\mathbf{x}) \;=\; -\sigma_l\, \mathcal{A}(\mathbf{x})\, N(\mathbf{x})\, l(\mathbf{x})\; \nabla V \cdot \langle \mathbf{e}_i \otimes \mathbf{e}_i \rangle_{\text{orientations}} \tag{3.8}$$

For a distribution corresponding with random orientation the averaging over all the orientations of $\langle \mathbf{e}_i \otimes \mathbf{e}_i \rangle$ is $\frac{1}{3}$ times the identity matrix. It is clear that because of the randomness the resulting matrix has to be proportional to the identity matrix. The $\frac{1}{3}$ is most easily calculated by noting that averaging over orientations the trace. Since the trace of $\mathbf{e}_i \otimes \mathbf{e}_i$ equals $\mathbf{e}_i \cdot \mathbf{e}_i$, the random averaging equals 1. The resulting expression for the macroscopic current density in a random orientated Plateau border network is

$$\begin{aligned} J(\mathbf{x}) &= -\frac{1}{3}\sigma_l\, \mathcal{A}(\mathbf{x})\, N(\mathbf{x})\, l(\mathbf{x})\, \nabla V \\ &= -\frac{1}{3}\, \sigma_l\, \Phi_\ell(\mathbf{x})\, \nabla V \end{aligned} \tag{3.9}$$

3.2 Electric conductivity and flow

The effective conductivity of a Plateau border structure is directly given by Eq. (3.9). The conductivity used there σ_l is the liquid conductivity. If the foam conductivity is compared to the liquid conductivity we get for the relative conductivity

$$\frac{\sigma_{foam}}{\sigma_l} = \frac{1}{3}\Phi_\ell. \tag{3.10}$$

This result was first derived in [8] and is therefore called the Lemlich limit for foam conductance. When films are participating in the conduction the Lemlich limit won't be valid any more. To handle this kind of problems we tried an effective-medium theory approach (§3.3).

The macroscopic flow $\mathbf{Q}(\mathbf{x})$ through a foam can be calculated in exactly the same way as the current density but instead of using Eq. (3.3) we use Eq. (3.11).

$$Q_i = -\frac{1}{C_{\text{disp}}\eta}\mathcal{A}_i^2 \nabla (p - \rho g z) \cdot \mathbf{e}_i. \tag{3.11}$$

This *flux* through a Plateau border equals the velocity (*Eq.* (2.9)) parallel to the Plateau border times its area $\mathcal{A}_i$. Now similar as in the case of the current density, a flow field can be constructed by the averaging procedure

$$\mathbf{Q}(\mathbf{x}) = -\frac{1}{3}\frac{1}{\eta^*}\mathcal{A}^2(\mathbf{x})\, N(\mathbf{x})\, l(\mathbf{x})\, \nabla (p - \rho g z)\,. \tag{3.12}$$

The main difference will be firstly that the flow depends quadraticly on the mean Plateau border area and not linearly like the electrical current density. Secondly the pressure which occurs in Eq. (3.12) depend via Laplaces law on the radius of curvature R (Eq. (2.1)) which is directly correlated to the area of the Plateau border (Eq. (2.2)). This gives an extra dependency on $\mathcal{A}(\mathbf{x})$ caused by the Laplace pressure $p(\mathbf{x})$. The flow expression will be used in chapter 4 to derive a equation governing drainage. It is the current density term in the continuity equation for the liquid fraction.

The Lemlich limit for the electric conductivity proves experimentally to be only very limited applicable because of the significant role liquid films can play for conduction at increasing liquid fractions. In the case of flow through a foam Eq. (3.12) is thought valid for a far larger range of the liquid fraction. Because of the viscous forces and the no slip boundary conditions the flow through the films will be neglected. This will be motivated more in §4.4.

3.3 permittivity and conductivity

When computing the effective conductivity we used the Plateau border network model. For calculating the effective permittivity we can't use this any more because of the non negligible permittivity of the gas phase. A second question concerns the contribution of the films. We will try to use effective-medium theory to approach the solution.

When the liquid fraction increases the structure of the foam will deviate from the simple Plateau border network structure. The Hashin-Shtrikman limits are the broadest limits between which the effective property of a randomly mixed binary structure has to lay, according to effective-medium theory. We will give them in the general case where σ_l and σ_g are the material properties of the liquid phase and the gas phase respectfully. Φ_ℓ and Φ_g are the liquid fraction and the gas fraction,

which add up to unity

$$\sigma_g + \frac{\Phi_\ell}{\frac{1}{\sigma_l-\sigma_g} + \frac{\Phi_g}{3\sigma_g}} \leq \sigma_{foam} \leq \sigma_l - \frac{\Phi_g}{\frac{1}{\sigma_l-\sigma_g} - \frac{\Phi_\ell}{3\sigma_l}}. \tag{3.13}$$

For the limiting case $\sigma_g = 0$ (electric conductivity) this gives

$$0 \leq \sigma_{foam} \leq \sigma_l \frac{\frac{2}{3}\Phi_\ell}{1 - \frac{\Phi_\ell}{3}}. \tag{3.14}$$

To derive an expression for the case of low liquid fractions Φ_ℓ we derive the Clausius-Mossotti formula. We will now switch from the language of conductivity to permittivity, because the physics is easier to picture in the language of only fields (electric displacement instead of current density). The mathematics, however is completely equivalent. We will use ε_l for the permittivity of the liquid phase and ε_g for the permittivity of the gas phase.

The Plateau borders and the films are abstracted as ellipsoids. The motivation for using ellipsoids is the technical convenience that their depolarising field is homogeneous when embedded in a homogeneous external field. For one ellipsoid in a homogeneous field $\mathbf{E}_g$, the internal $\mathbf{E}_l$ field obeys

$$\mathbf{E}_l = \mathbf{E}_g - \frac{\varepsilon_l - \varepsilon_g}{\varepsilon_g}\mathbf{L}\,\mathbf{E}_l \tag{3.15}$$

$$\mathbf{E}_l = \left(\mathbf{I} + \frac{\varepsilon_l - \varepsilon_g}{\varepsilon_g}\mathbf{L}\right)^{-1} \mathbf{E}_g \tag{3.16}$$

$\mathbf{L}$ is a matrix dependent on the geometry of the ellipsoid. In the coordinate system of the principle axes we find

$$\mathbf{L} = \begin{pmatrix} L_x & 0 & 0 \\ 0 & L_y & 0 \\ 0 & 0 & L_z \end{pmatrix} = \frac{1}{l_y l_z + l_z l_x + l_x l_y} \begin{pmatrix} l_y l_z & 0 & 0 \\ 0 & l_z l_x & 0 \\ 0 & 0 & l_x l_y \end{pmatrix}, \tag{3.17}$$

l_x,l_y and l_z are the lengths of the principal axes and Tr($\mathbf{L}$)=1. For a sphere all elements of $\mathbf{L}$ are $\frac{1}{3}$, for a needle directed in the z-direction we get

$$\mathbf{L} = \begin{pmatrix} \frac{1}{2} & 0 & 0 \\ 0 & \frac{1}{2} & 0 \\ 0 & 0 & 0 \end{pmatrix}. \tag{3.18}$$

An assumption one makes when deriving a Clausius-Mossotti formula is that the density of spheres is so scarce that they don't influence each other. In this limit the effective permittivity becomes

$$\varepsilon_{\text{foam}} = \frac{\varepsilon_g \Phi_g E_g + \varepsilon_l \Phi_\ell \langle E_l \rangle}{\Phi_g E_g + \Phi_\ell \langle E_l \rangle}. \tag{3.19}$$

Here is assumed that $\langle \mathbf{E}_l \rangle$ is parallel to $\mathbf{E}_g$ which we will proof in the case of random orientations of the spheres. A second assumption is that the dipole field

induced by the spheres in the gas phase will cancel out. This is true but won't be proven.

To get $\langle \mathbf{E}_l \rangle$ we have to rotationally average Eq. (3.16). Because $\mathbf{E}_g$ is constant we need to know

$$\beta = \left\langle \left(\mathbf{I} + \frac{\varepsilon_l - \varepsilon_g}{\varepsilon_g} \mathbf{L} \right)^{-1} \right\rangle_{\text{rotational}} . \tag{3.20}$$

In appendix B is proven that

$$\beta = \frac{1}{3} \mathrm{Tr} \left[\left(\mathbf{I} + \frac{\varepsilon_l - \varepsilon_g}{\varepsilon_g} \mathbf{L} \right)^{-1} \right] = \frac{1}{3} \left[\frac{1}{1 + \frac{\varepsilon_l - \varepsilon_g}{\varepsilon_g} L_x} + \frac{1}{1 + \frac{\varepsilon_l - \varepsilon_g}{\varepsilon_g} L_y} + \frac{1}{1 + \frac{\varepsilon_l - \varepsilon_g}{\varepsilon_g} L_z} \right] \tag{3.21}$$

In the following we will assume that $L_x = L_y = \frac{1}{2}(1 - L_z)$ leading to the Clausius-Mossotti formula for one randomly orientated structural element

$$\begin{aligned} \varepsilon_{\text{foam}} &= \frac{\varepsilon_g \Phi_g + \beta \varepsilon_l \Phi_\ell}{\Phi_g + \beta \Phi_\ell} \\ \beta &= \frac{1}{3} \left[\frac{4}{2 + \frac{\varepsilon_l - \varepsilon_g}{\varepsilon_g}(1 - L_z)} + \frac{1}{1 + \frac{\varepsilon_l - \varepsilon_g}{\varepsilon_g} L_z} \right] \end{aligned} \tag{3.22}$$

When $\varepsilon_g \to 0$, β will tend to zero for almost all L_z, and the effective permittivity will tend to zero (it is significant because $\sigma_g \to 0$ for conduction). There are only two exceptions $L_z = 0$ and $L_z = 1$. For these cases we have a singular limit of $\beta = \frac{1}{3}$ and $\beta = \frac{2}{3}$ respectably. The first case are ellipsoids deformed to cylinders (needles) and these can be associated with Plateau borders. The second case ($\beta = \frac{2}{3}$ for $\varepsilon_g = 0$) are ellipsoids deformed to plains (pancakes) these can be associated with the films. If we look upon the foam as random mixture of films and Plateau borders which do not influence each other (by dipole fields etc.), we can propose a mixing rule. We shouldn't linearly mix the effective permittivity for the films and the Plateau borders. Eq. (3.20) can be used, with also an averaging over the two kinds of structures. This will give

$$\beta_{\text{eff}} = \frac{\Phi_{\text{pb}}}{\Phi_\ell} \beta_{\text{pb}} + \frac{\Phi_{\text{film}}}{\Phi_\ell} \beta_{\text{film}}, \tag{3.23}$$

with

$$\begin{aligned} \beta_{\text{pb}} &= \frac{1}{3} \left[1 + \frac{4}{2 + \frac{\varepsilon_l - \varepsilon_g}{\varepsilon_g}} \right] \\ \beta_{\text{film}} &= \frac{2}{3} \left[1 + \frac{1}{2} \frac{1}{1 + \frac{\varepsilon_l - \varepsilon_g}{\varepsilon_g}} \right] . \end{aligned}$$

For $\varepsilon_g = 0$ we find for the effective property purely governed by the Plateau borders

$$\varepsilon_{\text{pb}} = \frac{1}{3} \frac{\Phi_\ell}{1 - \frac{2}{3}\Phi_\ell} \varepsilon_l . \tag{3.24}$$

It is promising to see that for low liquid fractions the limit of the Plateau border network model (the Lemlich limit) is reobtained.

In §5.3 we will try to use these expressions for the effective permittivity (and conductivity) to explain the measured calibration curves for the capacitance (and conductance) in relation to the liquid fraction. Here we hope to find what part of the liquid is in the films and what part is in the Plateau borders. The capacitance measurements have two intrinsic complicating factors compared to the conductance measurements. One is the non vanishing permittivity of the gas phase. The second is that there will always be a non zero conductance in the liquid phase due to ions etc.. To overcome this problem we can introduce complex conductivities σ_g^C and σ_l^C

$$\begin{aligned} \sigma_g^C &= i\omega\varepsilon_g \\ \sigma_l^C &= \sigma_l + i\omega\varepsilon_l. \end{aligned} \tag{3.25}$$

We here assume that the measurements are done in a alternating electric field with angular frequency ω, i.e. a harmonic oscillating field (time dependent factor $e^{i\omega t}$). This agrees exactly with our experimental setup. We can now apply the formulas for the effective conductivity. The end result will be a complex number. The phase factor is related to the phase difference between the electric field and the resulting current density. We are however interested in the in the amplitudes which is given by the absolute value of the complex conductivity.

The formulas derived here are not only applicable to electric phenomena, but also to for instance thermal conductivity in foams. It is especially useful to obtain the thermal conductivity in closed cell polyurethane foams. The mixing of the film, strut and gas contribution in this treatment different from the conventional one. In the conventional treatment the contributions of the three structural elements are computed separately and then a linear mixing rule is applied to get the resulting conductivity. The main lesson of effective-medium theory is, that you should be very careful in applying linear mixing rules. In the preliminary study given here we found that for low liquid fractions a linear mixing of the structural elements could be given for a parameter β (Eq. (3.24)). In the expression for the overall effective conductivity this β will both occur in the numerator and in the denominator. This is obviously no linear mixing rule.

In this chapter effective properties of the foam were described. We obtained two important results. The first was an expression for the flow through a network of Plateau borders. This expression will be used in the next chapter to derive an equation governing drainage. The second result was a more general effective-medium theory for dry foams. Although it has a wider use, in this report it will only be used to try to explain the conductance and capacitance measurements of a foam. These measurements have as primary goal to obtain calibration curves. We want to know the liquid fraction at a specific position in the foam column. This information is needed to verify the drainage model which will be derived in the next chapter.

Chapter 4

The drainage equation

Now the equation that governs flow through a network of Plateau borders will be given. We already derived an expression for the macroscopic flow through a foam in §3.2. All that has to be done is to substitute this flow in the continuity equation for the liquid fraction Φ_ℓ

$$\frac{\partial \Phi_\ell}{\partial t} + \nabla \cdot \mathbf{Q} = 0. \tag{4.1}$$

This then gives

$$\frac{\partial}{\partial t}\left[N(\mathbf{x},t)\,\mathcal{A}(\mathbf{x},t)\,l(\mathbf{x},t)\right] - \frac{1}{3\eta^*}\nabla\cdot\left[\mathcal{A}^2(\mathbf{x},t)\,N(\mathbf{x},t)\,l(\mathbf{x},t)\,\nabla\left(p-\rho g z\right)\right] = 0. \tag{4.2}$$

If we suppose that the Plateau borders density $N(\mathbf{x},t)$, and the mean length $l(\mathbf{x},t)$ are constants throughout space and time, we find

$$\frac{\partial \mathcal{A}}{\partial t} + \frac{1}{3\eta^*}\nabla\cdot\mathcal{A}^2\left(\rho g \mathbf{e}_z - \nabla p\right) = 0. \tag{4.3}$$

When we combine this with Eq. (2.2) and take the gas pressure in the bubble to be constant, we can express the pressure term in terms of $\mathcal{A}$.

$$\nabla p = -\gamma\sqrt{C_{area}}\nabla\frac{1}{\sqrt{\mathcal{A}}}. \tag{4.4}$$

Now a characteristic distance (x_0), and a characteristic time (t_0) can be introduced. The generic non-dimensional differential equation (for the non-dimensional Plateau border area α) is then given by

$$\frac{\partial}{\partial \tau}\alpha + \nabla\left[\alpha^2\left(\mathbf{e}_\zeta + \nabla\frac{1}{\sqrt{\alpha}}\right)\right] = 0. \tag{4.5}$$

The equation is generic because this formula contains no dimensionless parameters. Therefore it is valid for all foams independent of their material constants. The characteristic numbers are[1]

$$x_0 = \sqrt{\frac{\gamma}{\rho g}} \tag{4.6}$$

[1]Introduced in [15], without the factor 3 introduced by averaging.

$$t_0 = \frac{3\eta^*}{C_{area}}\sqrt{\frac{1}{\rho g \gamma}}.$$

In our experiments we will measure flow in a vertical tube filled with foam. Here the flow is essential one dimensional directed in the z-direction. The one dimensional version of the non dimensional equation describing this flow is

$$\frac{\partial}{\partial \tau}\alpha + \frac{\partial}{\partial \zeta}\left[\alpha^2\left(1 + \frac{\partial}{\partial \zeta}\frac{1}{\sqrt{\alpha}}\right)\right] = 0. \tag{4.7}$$

The connection to the physical variables and their dimensionless counterparts is given by

$$\begin{aligned} t &= t_0\,\tau \\ z &= x_0\,\zeta \\ u &= x_0/t_0\,v \\ \mathcal{A} &= C_{area}x_0^2\,\alpha. \end{aligned} \tag{4.8}$$

4.1 Mathematical Properties

The drainage equation Eq. (4.7) has three symmetry properties. The two most obvious ones are invariance under translation of τ and ζ, because Eq. (4.5) does not explicitly depend on them. There is however a third symmetry: if $\alpha(\tau, \zeta)$ is a solution, then

$$\lambda^2\,\alpha(\lambda^3\,\tau, \lambda\,\zeta) \tag{4.9}$$

is a solution too.

We will see that the drainage equation *Eq.* (4.7) has stable solitary wave solutions. The flow term directly gives that the velocity of the front of such a wave propagating through a initially completely dry foam wil have a dimensionless velocity $v = \alpha_{\text{wett}}$. α_{wett} is the non-dimensional liquid fraction established after the wavefront of the solitary wave. This is just a special case of a beautiful property: the *Sum law.* When a solitary wave is propagating through the foam, and the after the front the gradient $\frac{\partial \alpha}{\partial \zeta}$ is small, the associated non-dimensional flow is α^2. This means if one wave is catching up with an other wave, like depicted in Fig. 4.1, the difference of their flows is

$$\Delta J = \alpha_1^2 - \alpha_2^2.$$

The difference of their areas α is

$$\Delta\alpha = \alpha_1 - \alpha_2.$$

This is the area through which the catch-up wave is propagating. The associated catch-up velocity is

$$v = \frac{\alpha_1^2 - \alpha_2^2}{\Delta\alpha} = \alpha_1 + \alpha_2. \tag{4.10}$$

The velocity of the catch-up wave is the sum of the velocity of the wave being caught up and the velocity of the final wave.

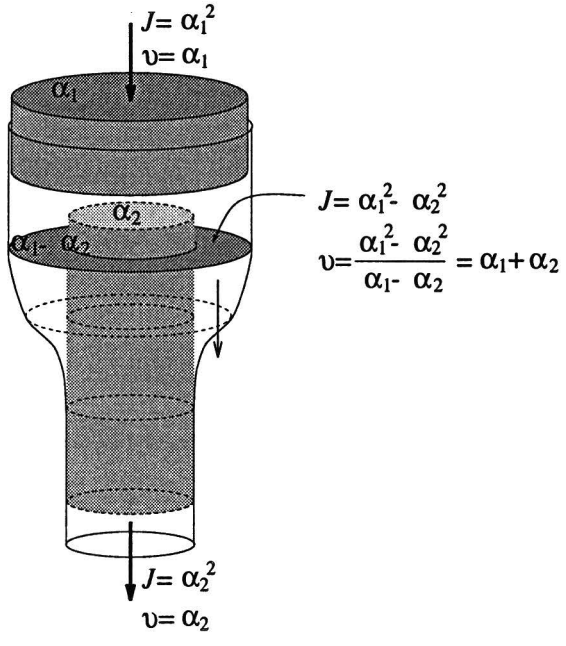

Figure 4.1: *Velocity of the catch-up wavefront. A very schematic picture of a solitary wave propagating through a strechable tube. This picture should not be seen as a vertical Plateau border. It only illustrates the gravitational term of the drainage equation. In fact, if we would take the pressure term in account for the depicted configuration we would get an instable situation (Rayleigh instability).*

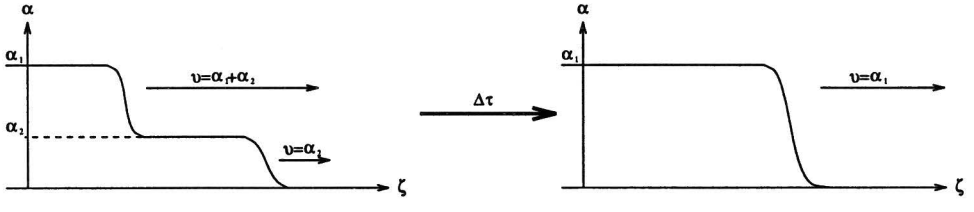

Figure 4.2: *Illustrating the Sum law. The velocity of the catch-up wave is the velocity of the wave its going to catch up plus the velocity of the wave once it is caught up.*

4.2 Analytic solutions

4.2.1 The solitary wave solution

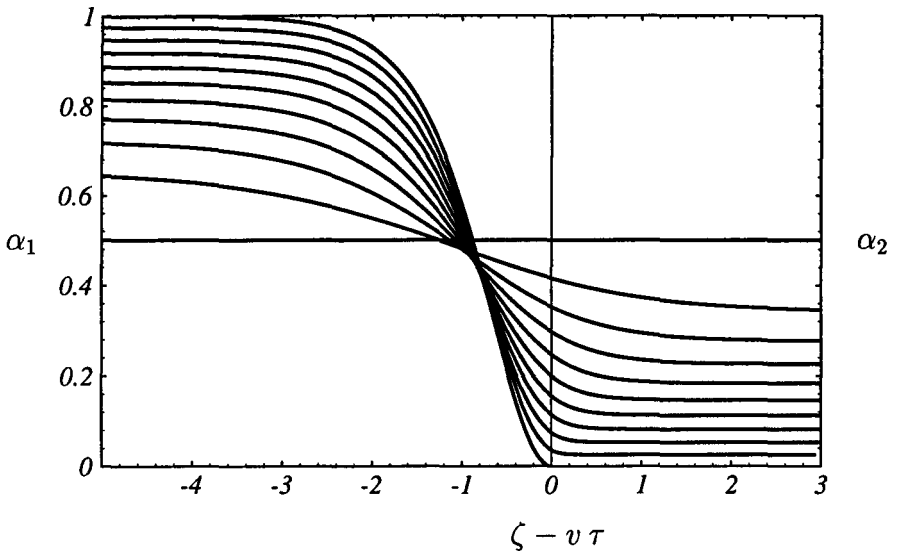

Figure 4.3: *Analytic solitary wave solutions propagating in a background α_2 with velocity $v = 1$. According to the sum law $\alpha_1 + \alpha_2 = 1$. All the other solitary wave solutions can be obtained by applying the symmetry properties.*

Results of experiments, similar to the ones described in this report, by D. Weaire *et al.* [18] pointed to the existence of solitary waves. Solitary waves that propagate with a constant velocity and preserve their form. When we substitute the solitary wave

$$\alpha(\zeta, \tau) = v f^2 \left[\sqrt{v}\,(\zeta - v\tau)\right] \tag{4.11}$$

and integrate Eq. (4.7) once, a solvable first order ordinary differential equation is found. The form of Eq. (4.11) may seem at first a bit awkward. The f^2 is introduced to lose the square root of Eq. (4.7) (this however gives the constraint $f > 0$, because we substituted $f = \sqrt{\alpha}$). Physically f^2 is proportional to the area of a Plateau border. The v (positive) stems from Eq. (4.11) and is introduced to lose the v-dependence in the resulting differential equation for f (Eq. (4.12)). The form is suggested by the symmetry property Eq. (4.9) ($\lambda = \sqrt{v}$). We obtain Eq. (4.12) by substituting Eq. (4.11) in Eq. (4.7) and integrating once

$$f^2(\xi) f'(\xi) - f^4(\xi) + f^2(\xi) = C_{int}, \qquad f > 0. \tag{4.12}$$

This then gives one integration constant C_{int}. In a indefinitely extended foam, a physical relevant solution obeys $f'(\xi) \to 0$ for $\xi \to \pm\infty$, which is only possible for $0 < C_{int} < \frac{1}{4}$. It can be shown by substituting $f'(\xi) = 0$ in Eq. (4.12) that

$$\alpha(-\infty, \tau) + \alpha(+\infty, \tau) = v, \tag{4.13}$$

which is equivalent to the sum law Eq. (4.10). This result is obtained in two steps, firstly solve the quadratic equation for f^2 one gets when $f' = 0$, this gives for the two solutions f_1^2 and f_2^2: $f_1^2 + f_2^2 = 1$. Secondly substitute this result in Eq. (4.11). This result is experimentally verifiable. The liquid fraction Φ_ℓ in the Plateau borders of a foam is proportional to α. The velocity of a drainage wave is proportional to v. If we could measure the liquid fraction as function of the height Eq. (4.13) would be very accessible. This will be shown in chapter 6.

Eq. (4.11) shows two characteristic dependencies on the velocity of the wave. Firstly the amplitude of the wave is proportional to the velocity, we have already discussed this. Secondly it shows that the width of the wave is proportional to $1/\sqrt{v}$, this means that the slower the wave (or equivalent the lesser its amplitude), the broader the wave front will be. This too will be tested experimentally (§6.3).

For $C_{int} = 0$ the solution to Eq. (4.12) is

$$\alpha(\zeta,\tau) = \begin{cases} v\ \tanh^2\left[\sqrt{v}(\zeta - v\tau)\right] & ,\ \zeta < v\tau \\ 0 & ,\ \zeta > v\tau. \end{cases} \tag{4.14}$$

When $C_{int} \neq 0$ an implicit expression for $f(\xi)$ exists

$$\begin{aligned} \xi_0 - \xi &= \frac{1}{\sqrt{1-4\,C_{int}}}\left[d_1 \operatorname{arctanh}\left(\frac{f}{d_1}\right) - d_2 \operatorname{arctanh}\left(\frac{d_2}{f}\right)\right] \\ d_1 &= \sqrt{\frac{1}{2} + \frac{1}{2}\sqrt{1-4\,C_{int}}} \\ d_2 &= \sqrt{\frac{1}{2} - \frac{1}{2}\sqrt{1-4\,C_{int}}}. \end{aligned} \tag{4.15}$$

To obey Eq. (4.15) f has to satisfy $d_2 < f < d_1$ ($-d_1 < f < -d_2$ would be valid too but $f > 0$ according to Eq. (4.12)). If $f \to d_2$ then $\xi \to \infty$ and if $f \to d_1$ then $\xi \to -\infty$. This solution transforms to Eq. (4.14) for $C_{int} \to 0$

$$\xi_0 - \xi = \operatorname{arctanh}(f) - \sqrt{C_{int}}\operatorname{arctanh}\left(\frac{\sqrt{C_{int}}}{f}\right). \tag{4.16}$$

This gives for

$$\begin{aligned} \sqrt{C_{int}} < f < d\sqrt{C_{int}} \ &\Rightarrow\ -\infty < \xi_0 - \xi < 0 \\ d\sqrt{C_{int}} < f < 1 - C_{int} \ &\Rightarrow\ \xi_0 - \xi = \operatorname{arctanh}(f) + O(\sqrt{C_{int}}), \end{aligned} \tag{4.17}$$

with

$$\frac{1}{d} = \tanh d,\ d = 1.20,$$

and this way illustrating the transformation.

Eq. (4.12) has other singular solutions. These solutions can't be identified with solitary waves because they are only valid on a range which is bounded at one or both sides, preventing a indefinite (x,t)-range in Eq. (4.11). However physical

situations can be imagined where they arise, e.g; a the stationary curve of a foam in a tube which is created at the bottom and collapses at some height. Here the flow in the foam downward is $\alpha^2\left[1+\frac{\partial}{\partial\zeta}\frac{1}{\sqrt{\alpha}}\right]$. The flow associated with the foam flowing upward is $v\,\alpha$. This has the extra assumption that the foam bubbles are incompressible. Because of stationarity α depends only on ζ and the continuity equation gives

$$\frac{d}{d\zeta}\left(\alpha^2\left[1+\frac{d}{d\zeta}\frac{1}{\sqrt{\alpha}}\right]-v\,\alpha\right)=0. \tag{4.18}$$

This can be reduced to Eq. (4.12). There is no physical reason why the interval of ζ shouldn't be bounded, and the singular solutions can arise. The complete solutions can be derived by alternatively interchanging the "arctanh" terms with "arccoth" terms. Terms with "arctan" and "arccot" will emerge when other values of C_{int} are introduced and complex quantities emerge in the "arctanh" and "arccoth" functions.

4.2.2 The static case

In the static case the flow is zero everywhere, the pressure gradient is equal in magnitude but opposite in sign to ρg, so

$$\alpha^2\left[1+\frac{\partial}{\partial\zeta}\frac{1}{\sqrt{\alpha}}\right]=0. \tag{4.19}$$

This results in

$$\alpha=\frac{1}{(\zeta_0-\zeta)^2},\ \zeta<\zeta_0. \tag{4.20}$$

4.2.3 The stationary case

In the stationary case the flow is constant (J)

$$\alpha^2\left[1+\frac{\partial}{\partial\zeta}\frac{1}{\sqrt{\alpha}}\right]=Q. \tag{4.21}$$

Besides the obvious solution

$$\alpha=\sqrt{Q}, \tag{4.22}$$

it has ζ dependent solutions. With $\alpha(\zeta)=Q^{\frac{1}{2}}f^2\left(Q^{\frac{1}{4}}\zeta\right)$, this gives for $f(\zeta)$

$$\zeta-\zeta_0=\frac{1}{2}\arctan(f)-\frac{1}{2}\operatorname{arctanh}(f),\ 0<f<1. \tag{4.23}$$

or

$$\zeta-\zeta_0=\frac{1}{2}\arctan(f)-\frac{1}{2}\operatorname{arccoth}(f),\ 1<f<\infty. \tag{4.24}$$

Both the stationary and the static curve can be found by applying the right limiting procedure to the solutions of Eq. (4.12).

4.3 Free drainage and pulses

It is a small miracle that the drainage equation, despite its non-linearity has relative simple analytic solutions. For describing free drainage and pulses we haven't found exact results. It is therefore inevitable to use some approximation. The treatment here will be to use the equation without the pressure term. Subsequently we will try to estimate the deviation from the full solution of the drainage equation and will if possible compensate for it. The deviations won't be rigorous and not all steps are fully motivated. Part of the justification are computer simulations of the drainage and experimental results.

The equation without the pressure term is the most simple quasi-linear partial differential equation, and much is known about it

$$\frac{\partial}{\partial \tau}\alpha + \frac{\partial}{\partial \zeta}\alpha^2 = 0. \tag{4.25}$$

The equation has been studied this well because it is not only the limiting case of the drainage equation but also of the Burgers equation. This equation, having soliton solutions reduces to Eq. (4.25) if we discard the second order terms. The implicit solution of it is known

$$\alpha = f(\zeta - 2\alpha\tau), \tag{4.26}$$

this solution is easily found by the use of the Method of Characteristics. The initial values are given by $\alpha(\zeta, 0) = f(\zeta)$, and the characteristic curves by

$$\zeta(\tau) = 2f(\zeta_0)\tau + \zeta_0. \tag{4.27}$$

The solution breaks down if these characteristic lines intersect. Supposing the initial values were sufficiently smooth, this will happen at time

$$\tau_{shock} = \mathrm{Min}\frac{-1}{2f'(\zeta)}, \tag{4.28}$$

then a singularity (a shock wave) will be formed which will propagate with a velocity

$$v_{shock} = \alpha_+ + \alpha_- \tag{4.29}$$

The solution with singularities can be constructed by using Eq. (4.26). This solution may be multivalued, these parts are cut off in such a way that the total area beneath the curve stays the same as illustrated in Fig. 4.5. This is a bit like the procedure one uses when calculating the phase diagram of a van der Waals gas. There the total area beneath the unstable domain has to stay the same because of conservation of energy. Here we have to obey the conservation of the amount of liquid as demanded by the continuity equation for the liquid fraction. When the initial curve ($t = 0$) is only nonzero at a interval $[0, \Delta\zeta]$ (a pulse), we construct by using the implicit solution (Eq. (4.26)), only nonzero values for α if

$$\begin{aligned} 0 < \quad & \zeta - 2\alpha\tau \quad < \Delta\zeta \\ \frac{\zeta - \Delta\zeta}{2\tau} < \quad & \alpha \quad < \frac{\zeta}{2\tau} \end{aligned} \tag{4.30}$$

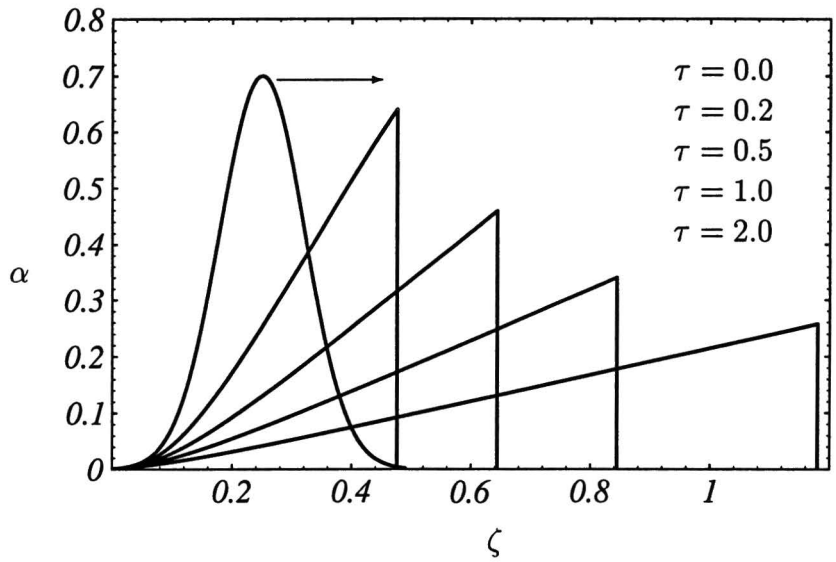

Figure 4.4: *The creation of a sawtooth wave.*

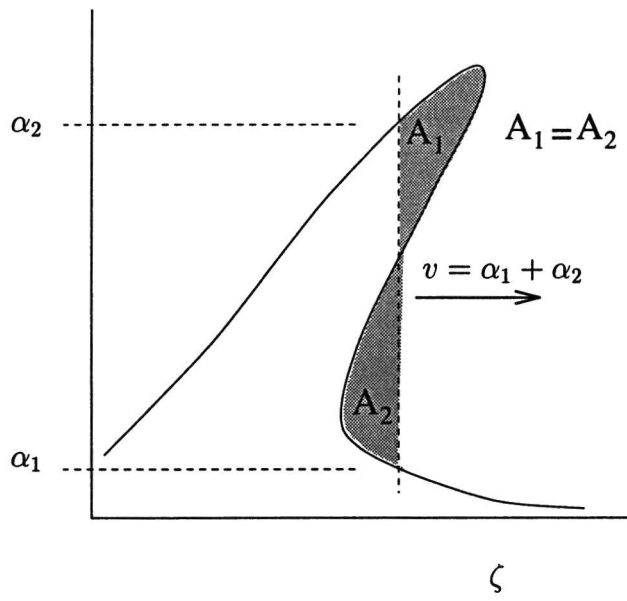

Figure 4.5: *The procedure to get the singular shock wave solution, when knowing the implicit multivalued solution.*

If we now apply the cutoff procedure described above, we see that a pulse for longer times always will approximate a "saw tooth" shape. The position of the top of the sawtooth wave will be approximately

$$\begin{aligned} \zeta_{top} &= 2\sqrt{Vt} \\ \alpha_{top} &= \sqrt{\frac{V}{t}} = v_{top}. \end{aligned} \tag{4.31}$$

Here V is the total volume under the graph (the total amount of liquid) which has to be conserved $V = \int \alpha d\zeta$.

Free drainage can be modeled with as initial profile a step wave Fig. 4.6. This

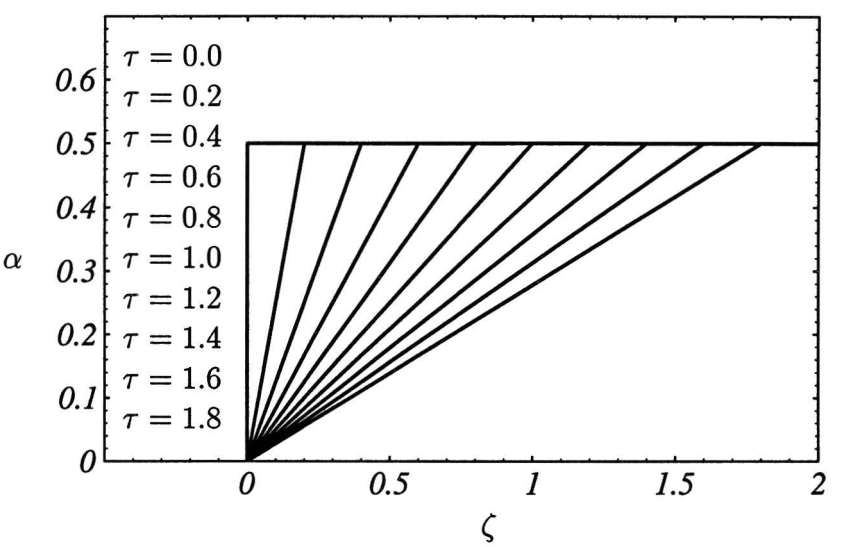

Figure 4.6: *Free drainage if only the gravitational term is taken into account.*

is still easier to model because the implicit solution does not break down. Here too is a linear tail. The transition between this tail and the horizontal piece propagates with a velocity of 2α. The slope will evaluate in time as

$$\text{slope} = \frac{1}{2\tau}. \tag{4.32}$$

For the solutions of Eq. (4.25) we can make the following observations

- The propagating velocity of a non singular piece of the curve is 2α (substitude $f \rightarrow \alpha$ in Eq. (4.26)).
- Negative slopes are unstable and will give rise to singularities, e.g; Fig. 4.4.

- After some time sawtooths will emerge. The time behaviour of their slopes is $\frac{1}{2(\tau+\tau_0)}$, e.g; Fig. 4.6.
- To calculate the singular fronts: use conservation of area beneath the curve Fig. 4.5.

The difficult part in analysing pulses and free drainage profiles is the role of the pressure term. The flow associated with the pressure term counteracts gradients. This is depicted in Fig. 4.8. It will diffusively eliminate little bumps and will soften the large gradients (the singularities) caused by the gravitational term (Fig. 4.4). The next matter which we will address is whether there will be intervals where the pressure term is insignificant and the character of the solutions without this term, described above will become apparent. If we suppose there is a pulse or a free drainage profile, with the typical time dependence of the slope of its tail of $\zeta/2\tau$, it can survive for long times. To survive the pressure term should be negligible compared to the gravitational term, so

$$\begin{aligned} \alpha^{\frac{1}{2}}\frac{\partial \alpha}{\partial \zeta} &\ll \alpha^2 \\ \zeta &\gg \tau^{\frac{1}{3}}. \end{aligned} \tag{4.33}$$

This constraint can be met for long times because in the case of free drainage profile the transitional area will propagate with a constant velocity, so there will come a time were Eq. (4.33) can be met. In the case of a pulse the position of the top is proportional with the square root of τ Eq. (4.31). for long times an area will evolve where Eq. (4.33) is met although for pulses the constraint is more stringent. This is illustrated in Fig. 4.3.

The pressure term makes the differential equation a second order equation implying a need for two boundary conditions. For example one at the top of the foam and one at the bottom. When describing free drainage we had only a boundary condition at the top: the flow should be zero at the top, which was equivalent with $\alpha = 0$. Now this constraint will become

$$J = \alpha^2 - \frac{1}{2}\sqrt{\alpha}\frac{\partial \alpha}{\partial \zeta} = 0. \tag{4.34}$$

The second boundary condition at the bottom is more difficult. In general the foam column will rest on the liquid. But near the liquid our model will break down, because its a model for low liquid fractions. The constraint we used in simulations of free drainage was to set the liquid fraction equal to some critical liquid fraction were you would expect the model to break down. A bounding limit for the liquid fraction is for example the Bernal packing fraction of spheres ($\Phi_\ell \approx 0.3$). The most simple approximation to evaluate the part of the free drainage profile where the gravitational term governs the behaviour is just to assume that the slope dependence and extrapolate this solution to the top of the foam and then apply Eq. (4.34) (proposed in [17]).

$$\alpha(\zeta, \tau) = \frac{\zeta}{2\tau} + \alpha(0, \tau) \tag{4.35}$$

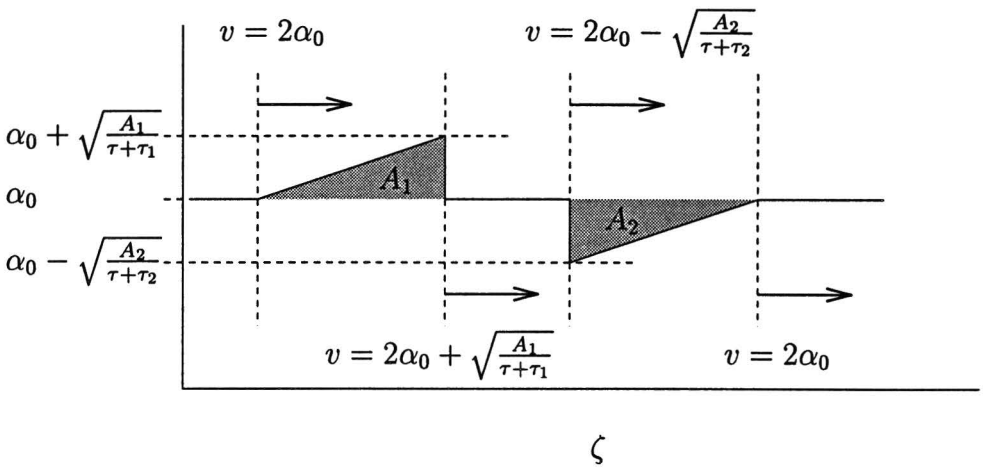

Figure 4.7: *Pulses on a background.*

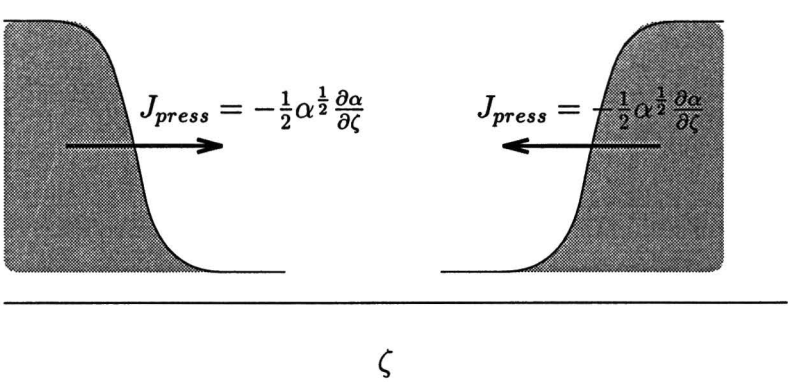

Figure 4.8: *The pressure term counteracts gradients in the liquid fraction.*

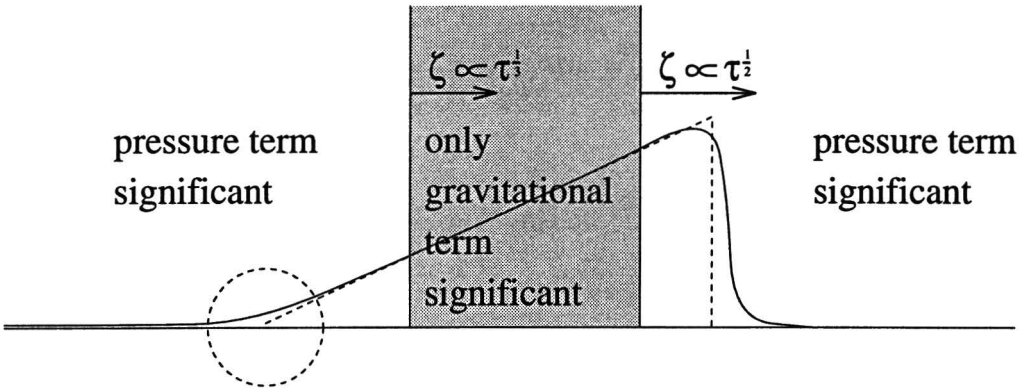

Figure 4.9: *linear piece where only the gravitational term is significant*

$$\alpha^2(0,\tau) - \frac{1}{2}\sqrt{\alpha(0,\tau)}\,\frac{1}{2\tau} = 0$$
$$\alpha(0,\tau) = (4\tau)^{-\frac{2}{3}}.$$

4.4 Validity, stability and perturbations

When setting up the model we made some assumption. Here, these assumptions are summed up to give a good insight into the validity of the model and into its limitations.

- The liquid fraction in the foam has to be low enough so the Plateau borders are the structures that determine the flow. We will try to estimate for what liquid fractions the film contribution are neglegible. Let Φ_{pb} be the liquid

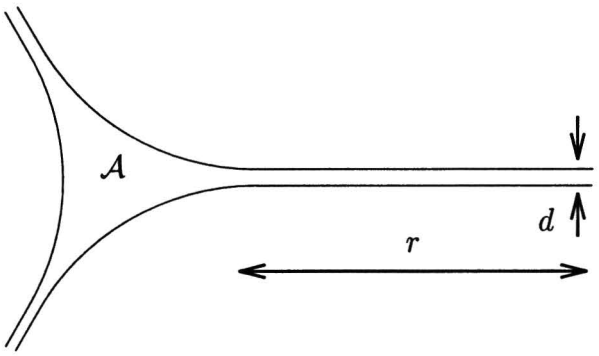

Figure 4.10: *A Plateau border and a film*

fraction situated in the Plateau borders and Φ_{film} the liquid fraction situated in the films. We will model the bubbles as Kelvin cells (see §6.1), with edges

of length l. Plateau borders are associated with these edges. The cell has 36 edges all shared with two others. We describe the films as a shell with width d around The total volume is $8\sqrt{2}\,l^3$.

$$\begin{aligned} \Phi_{\text{pb}} &= \frac{3\sqrt{2}}{4}\frac{\mathcal{A}}{l^2} \\ \Phi_{\text{film}} &\approx \frac{d}{l} \end{aligned} \tag{4.36}$$

We will compare the Poiseuille flow in a vertical Plateau border and in a vertical liquid film with the typical dimensions of $l \times l$ as depicted in Fig. 4.4 We will take the film to have a rectangular cross area. This gives for the flow in the film (Q_{film}), with $d \ll l$

$$Q_{\text{film}} = \frac{1}{12} l d^3 \times \rho g. \tag{4.37}$$

When comparing the flux through a Plateau border and to the film we can estimate it as

$$\frac{Q_{\text{pb}}}{Q_{\text{film}}} = \frac{12}{49.6}\frac{\mathcal{A}^2}{l^3 d} \approx 0.3 \times \frac{\Phi_{\text{pb}}^2}{\Phi_{\text{film}}}, \tag{4.38}$$

by using Eq. (2.6) and using the right expressions for the Plateau border. When the foam is dry the films are sucked empty by the Plateau borders and there will be no flow at all. A typical thickness of a film is 1 μm. This gives a very low liquid fraction in the films ($\Phi_{\text{film}} \approx 10^{-3}$). When the foam is in a transition state the films will swell up. If it is possible to find out the liquid fraction in the films we now have a rough estimation for the validity of the model. To be still valid the quotient Eq. (4.38) should be at least larger then 1.

- The characteristic length scale (x_0) is larger then the Plateau border length. This assumption was needed to be able to use the average procedure. It gives a very easy experimentally verifiable criterion (using Eq. (4.6))

$$\sqrt{\frac{\gamma}{\rho g}} \gg R_{bubb} \tag{4.39}$$

We used the bubble radius R_{bubb} because it is approximately the same length as the Plateau border. If this criterion is not met this does not mean that profiles do not obey the theory. If the width of a profile is much greater than the bubble radius there is still no problem. The criterion just indicates that it is very well possible that typical profiles (such as the static profile) have too small a width to be treated by the theory.

- We supposed no-slip boundary conditions. It is unclear whether this is a valid assumption. It is very dependent on what kind of surfactant is used and on the viscosity of the fluid.

- When we derived the drainage equation we supposed that the number of Plateau borders N and their lengths l were both independent of space and time. If we start with a homogeneous blown foam, this is equivalent to saying that the foam structure is completely rigid. This is not true of course, but in the limit of low liquid fractions the effects are small compared to changes in the Plateau border area $\mathcal{A}$. We can associate with a bubble a specific number of Plateau borders. When the bubbles are compressed, the number of bubbles per unit volume increases and therefore N will increase. Lets suppose the gas in the bubbles is incompressible. If the liquid fraction increases, the number of bubbles per unit volume therefore decreases and N decreases. The number of bubbles per unit volume N_{bubb} is then

$$N_{bubb} = \frac{1 - \Phi_\ell}{V_{bubb}}, \tag{4.40}$$

with V_{bubb} the volume of a bubble. If we suppose the length of a Plateau border is directly related to the volume of the bubble, which is unchanged, we get

$$\Phi_\ell = \frac{N_0 l_0 \mathcal{A}}{1 + N_0 l_0 \mathcal{A}}, \tag{4.41}$$

N_0 is the number of Plateau borders per unit volume and l_0 their length. When the liquid fraction increases the foam becomes heavier. If the foam column rests on a liquid (like in our experiments) a part of its total height will be beneath the liquid surface (see Fig. 5.7). When it is uniformly wetted, this part will be equal to the liquid fraction Φ_ℓ, and a fraction $1 - \Phi_\ell$ will be above the water. If the bubbles are incompressible the foam will be expanded with a factor $1/(1 - \Phi_\ell)$, so when wetted the height of the part of the foam above the liquid surface will always remain the same. Inversely, if in an experiments the top of the foam keeps the same position the bubbles can be treated as incompressible.

- The curvature of the Plateau border in the longitudinal direction has to be negligible compared to curvature perpendicular. This can of course only be true when the liquid fraction is low enough and the Plateau borders can be looked upon as tubes. A second and closely related restriction is that the Plateau borders are to a good approximation straight. If this is not satisfied we can not use Poiseuille flow in a tube. These two restrictions give the (non dimensional) criteria

$$\left|\frac{\partial R}{\partial z}\right| < 1 \qquad \left|\frac{1}{R}\frac{\partial^2 R}{\partial z^2}\right| < 1 \;\rightarrow \tag{4.42}$$
$$\left|\frac{\partial \alpha}{\partial \zeta}\right| < \sqrt{\alpha} \qquad \left|\frac{\partial^2 \alpha}{\partial \zeta^2}\right| < 1$$

Here R is the radius of curvature. This radius is not allowed to vary to quickly, because this would introduce curvature parallel to the Plateau borders, which we neglected in our model. These criteria restrict the valid

solutions of the differential equation Eq. (4.7). For example for a solitary wave it is equivalent to demanding that the dimensionless velocity $v \ll 1$. In §6.1 we will seen this criterion is met.

- Flow in a vertical tube filled with foam can be treated as one dimensional. The flow in the horizontal plane is also governed by Plateau borders, there the gravity plays no role and only pressure differences are the driving forces. According to Eq. (2.1) (assuming that all bubbles are the same pressure) this means liquid will flow from larger Plateau borders to smaller ones. It is therefore a good assumption that a uniformity in the Plateau border sizes in the horizontal plane will develop and persist. That the Laplace pressure not always leads to a homogeneous size distribution is shown in the case of soap froths. Large bubbles will have a smaller curvature and therefore a smaller Laplace pressure then small bubbles. Gas diffusion between the bubbles will go from small to larger bubbles. A soap froth is always unstable. For an aging foam the assumption that all bubbles have the same size and same pressure will therefore no longer be true. It is evident however that the characteristic time for gas diffusion is much larger then the characteristic time for equilibration in the horizontal plane by flow through Plateau borders. In the experiments, we used fresh blown foams and the problem did not occur.

Above we remarked that the pressure term of the flow smooths bumps. This becomes even more clear if we linearise the drainage equation around a steady drainage profile α_0 (= constant).

$$\alpha(\zeta, \tau) = \alpha_0 + \epsilon\tilde{\alpha}(\zeta, \tau), \tag{4.43}$$

where ϵ is a small parameter for which we expand to first order The linearised equation becomes

$$\frac{\partial}{\partial\tau}\tilde{\alpha} + 2\alpha_0\frac{\partial}{\partial\zeta}\tilde{\alpha} - \frac{\sqrt{\alpha_0}}{2}\frac{\partial^2}{\partial\zeta^2}\tilde{\alpha} = 0. \tag{4.44}$$

The second gravitational term is a translational term with a velocity of $2\alpha_0$ what is a under bound of the sum law ($v = v_a + v_b > 2v_a$). The third term, the pressure term, is as expected a diffusive term. The general solution of Eq. (4.44) is

$$\tilde{\alpha}(\zeta, \tau) = \frac{1}{\sqrt{2\pi\,\tau\sqrt{\alpha_0}}}\int d\tilde{\zeta}\ \tilde{\alpha}(\tilde{\zeta}, 0)\ \exp\left[-\frac{(\tilde{\zeta} - \zeta - 2\alpha_0\tau)^2}{2\tau\sqrt{\alpha_0}}\right] \tag{4.45}$$

The Green's function is a typical one characterising diffusion. It is a Gaussian curve that translates with a velocity 2α, its width increases with the square root of the time ($\sqrt{\tau}$) (the diffusion constant is $\sqrt{\alpha}/2$).

Systems that combine flow and surface tension are famous for their Rayleigh instabilities. For example a flow with a circular cross section can become instable. The curvature longitudinal to the cylinder stabilises the flow. The curvature perpendicular on that destabilises the flow. The reason is very similar to that of the instability of a foam froth. When the circular cross section increases, its curvature decreases and so its Laplace pressure decreases. Therefore if the curvature

in the longitudinal direction is small the pressure will be the smallest where the cross section is the greatest. This is clearly an unstable situation. In the case of a Plateau border however even this second curvature has a stabilising character. This is so because a larger Plateau border is associated with a larger curvature (less negative). We have studied the second curvature term and which became a very tedious expression. We even performed some computer simulations with an approximate, simplified expression. When this curvature is taken account the expression for the Poiseuille flow should also be altered because the tube is not a straight Plateau border any more. This complicates the mathematics enormously. Here we no describe this study as its outcome mainly focused on the mathematics and numerics involved, no real physical insight was gained.

Chapter 5

The Measurement Apparatus

In this report the liquid fraction in a foam is measured with a *level gauge.* This apparatus was originally developed by K.S.L.A. to measure the petrol level in underground fuel storage tanks for retail stations. It has previously been used to study oil-water interfaces as well as oil dehydration.

This was all done with a capacitance version of the level gauge. During this traineeship a new version of the level gauge has been developed by J. van der Steen [14]. Instead of measuring the capacitance, the conductance is measured. This gauge was especially designed for foam studies. Because it is new and not well described yet, the emphasise will be on the conductance level gauge which is explained in more technical detail than the capacitance level gauge.

The level gauge is a segmented apparatus: it has a spatial resolution. To measure foam drainage with a spatial resolution is new. The classical way of measuring foam drainage was done by measuring the outflow of liquid out of the foam as a function of time. We now have a method to look at the liquid fraction of the foam in the vertical direction and as function of time. This obviously has great advantages and facilitates the study of drainage mechanisms.

5.1 Capacitance measurements

The used level gauges consist of 54 segments at one side and a few larger plates on the other side of the column (Fig. 5.3). The segment size is of the order of $1 \times 1\text{cm}^2$. Each time step (larger than 2.5 seconds) the capacitance is measured for each individual segment. Fig. 5.3 depicts a level gauge. In the ideal case of capacitance or conductance measurement, one would apply an alternating potential on the large plate and connect the measurement segments with virtual zero using a opamp as depicted in Fig. 5.2 for one element. When we apply a alternating potential U_i and angular frequency ω, ideal electronics would give us a output (complex) potential of

$$\begin{aligned} U_o &= \frac{R_f A}{L}(\sigma + i\omega\varepsilon)U_i \\ |U_o| &= \frac{R_f A}{L}\sqrt{\sigma^2 + \omega^2\varepsilon^2}|U_i|. \end{aligned} \tag{5.1}$$

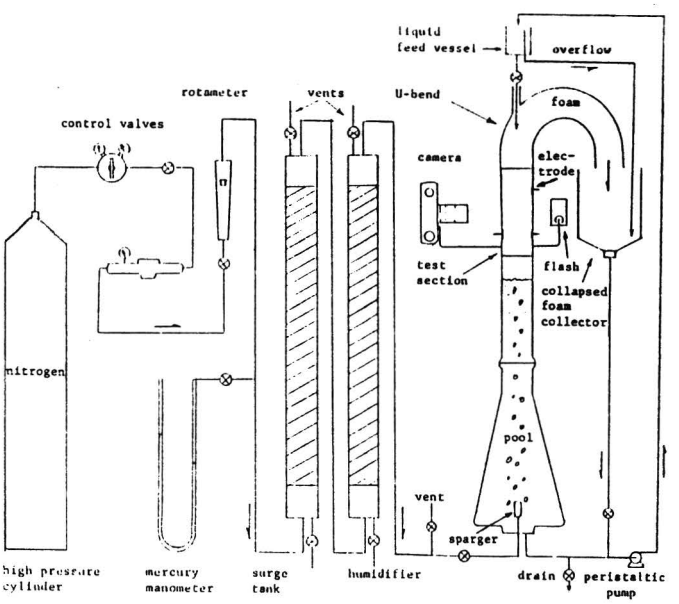

Figure 5.1: A classical foam drainage experiment

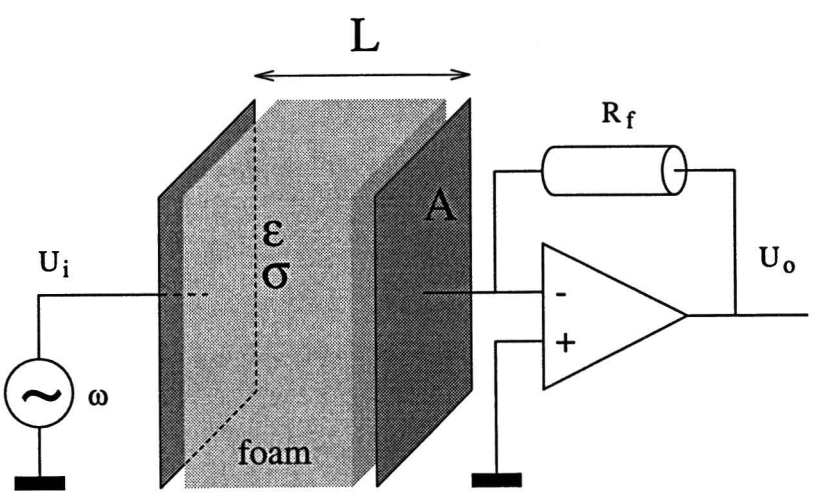

Figure 5.2: *An ideal measurement of the effective dielectric constant.*

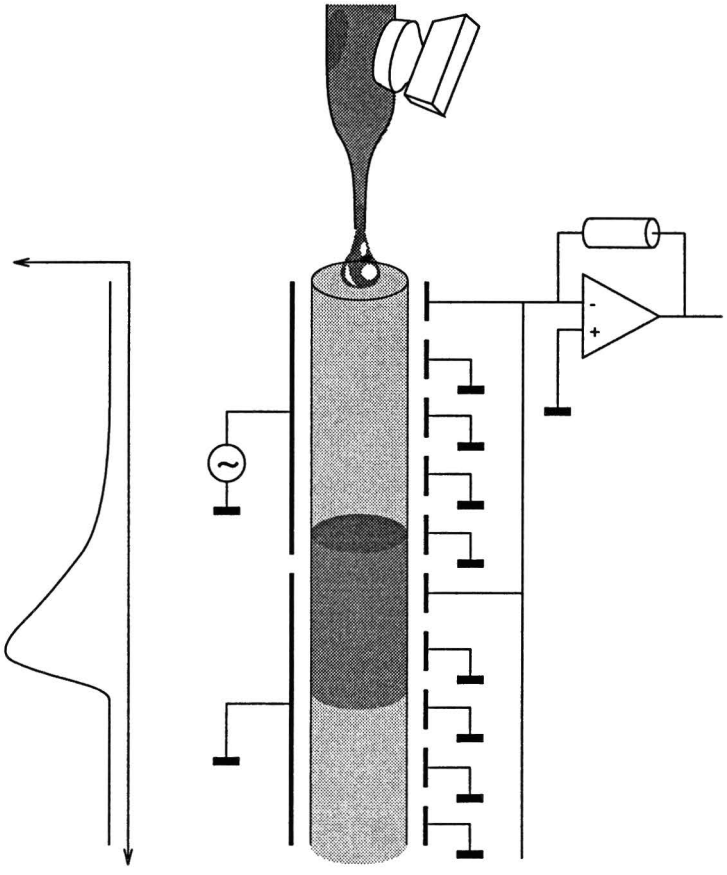

Figure 5.3: *A schematic setup of a drainage experiment using a level gauge*

When we define

$$\omega_{crit} = \frac{\sigma}{\varepsilon}, \tag{5.2}$$

we demand that $\omega \gg \omega_{crit}$ to have a good capacitance measurement and that $\omega \ll \omega_{crit}$ for a good conductance measurement.

The capacitance measurement has many more non-idealities as the conductance measurements. This makes it very hard to give a model for the obtained capacitance as function of the liquid fraction in a foam. We already have mentioned some difficulties which had to do with the effective permittivity in §3.3 (namely the non negligible gas phase and possible conductivity). The other difficulties are on the one hand inherent to capacitance measurements, on the other hand they could have been much reduced if the gauge would have been designed for this particular foam application. The main goal in the design wasn't a high precision instrument, but a gauge usable for the above mentioned commercial purposes. In Fig. 5.4 two nonidealities are depicted: the first is a typical one related to capacitance measurements, the second one was due to the non-optimal geometry of this test gauge, and would not be there if the gauge was made for laboratory purposes. The capacitance measurements were done on a foam contained in a round plastic tube (see Fig. 5.3). All the material between the electrodes and the foam have

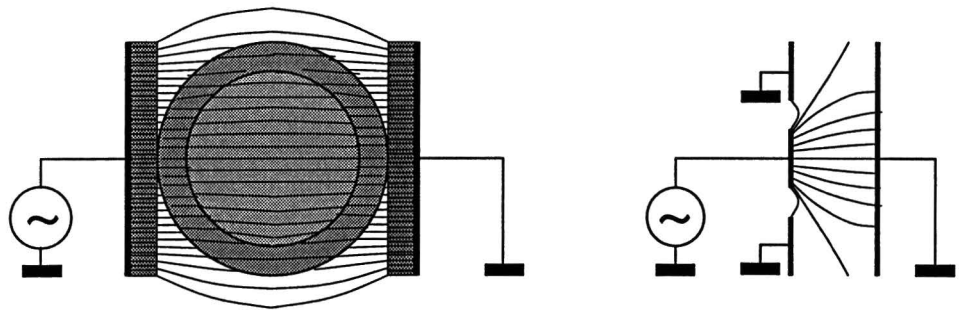

Figure 5.4: *Two non idealities. Firstly: parasitic capacitances due to the tube and the geometry. Secondly: the smaller segments instead of the larger plates are connected to the source, causing a more inhomogeneous field.*

parasitic effects. Because of the finite size of the segments and the non rectangular cross section of the tube the electric field will not be homogeneous, and the foam will not be optimally sampled. If we simplify the problem to its extreme we can look upon the problem as a parasitic capacitance C_{par} and a capacitance caused by the foam C_{foam} in series. This gives for the total capacitance C_{tot}

$$\begin{aligned} \frac{1}{C_{\text{tot}}} &= \frac{1}{C_{\text{par}}} + \frac{1}{C_{\text{foam}}} \\ C_{\text{tot}} &= \frac{C_{\text{par}}}{1 + \frac{C_{\text{par}}}{C_{\text{foam}}}} \end{aligned} \tag{5.3}$$

It is clear that if C_{foam} becomes larger then C_{par} the value of C_{foam} decreases to attribute to the measured signal (which is proportional to C_{tot}). To make a estimation we could linearise the Clausius-Mossotti formula (Eq. (3.22)) for low liquid fraction and derive for which fraction C_{foam} exceeds C_{par}. We estimate $C_{\text{foam}} \approx \frac{A}{D_{\text{tube}}}\left(\varepsilon_g + \frac{1}{3}\varepsilon_l \Phi_\ell\right)$, with A the area of the electrode and D_{tube} the diameter of the tube ($\approx$ 2cm). This gives a critical liquid fraction

$$(\Phi_\ell)_{\text{crit}} = \frac{D_{\text{tube}} C_{\text{par}}}{A(\varepsilon_g + \frac{1}{3}\varepsilon_l \Phi_\ell)}, \tag{5.4}$$

We have for water $\varepsilon_l \approx 80\varepsilon_0$, for the gas $\varepsilon_g \approx 1\varepsilon_0$ and for perspex $\varepsilon_{\text{perspex}} \approx 4\varepsilon_0$. Because the permittivity of water is so large, compared to perspex and air the tube and isolation material of a few millimeters can influence the precision of the capacitance measurements. We will see this in §5.3 when we discuss the calibration curves.

In the next section the multiplexing used in the conductance level gauge will be discussed. We already touched upon the fact that in the capacitance level gauge the field is inhomogeneous, because of the unfortunate choice of connecting the smaller segments to the source. When the distance between the two segmented plates becomes of the same order of magnitude as the plate that carries the source potential inhomogeneity of the field will start to occur. In the conductance level

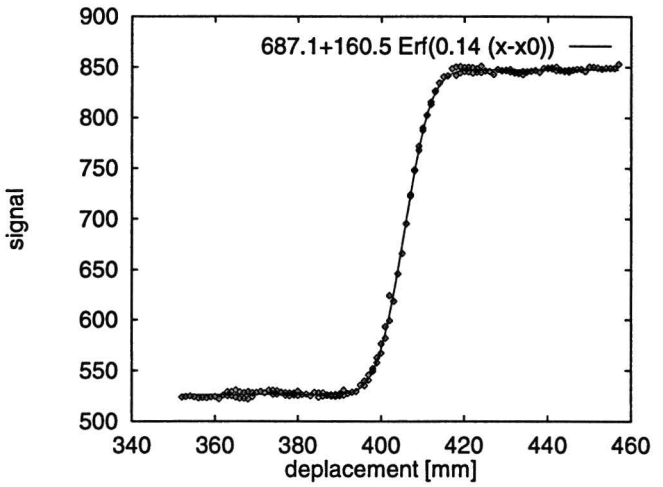

Figure 5.5: *Broadening caused by a step in the dielectric constant electric field.*

gauge the larger plates are connected to the larger source plates and all the segments are connected to ground (or virtually ground). The inhomogeneities are small because the plates are larger the the diameter of the tube.

When introducing a step in the permittivity this will also cause some extra broadening in the profile. Even in a homogeneous external field the resulting field will be inhomogeneous due to the inhomogeneous depolarising field. To investigate what kind of broadening one will measure when measuring a sharp profile, we used a glass rod for establishing a perfect step in the permittivity. This measurement (Fig. 5.5) can be fitted very well with an error function suggesting Gaussian broadening. When measuring sharp drainage profiles this broadening has to be taken into account.

5.2 Conductance measurements

The conductance level gauge was especially developed to do foam measurements. This means more care was taken to guaranty precision and linearity of the response (linearity between the response and the resistance measured). With given sensor geometry, the range of the measured conductance went up to $1.2\text{k}\Omega^{-1}$, with a precision for low conductances of at least $1\text{M}\Omega^{-1}$. We used ordinary tab water with a non ionic surfactant (dobanol). For a very dry foam we measured $6\text{M}\Omega^{-1}$, hundred percent liquid gave approximately $550\text{M}\Omega^{-1}$. The electrodes for this conductance measurements are in direct contact with the foam, therefore there are much less parasitic effects.

Electronics behave never completely ideally and in this measurement this becomes most often apparent if one wants to measure extremes like steps from high resistances to low resistances (e.g. from a dry foam to a aqueous foam). To give

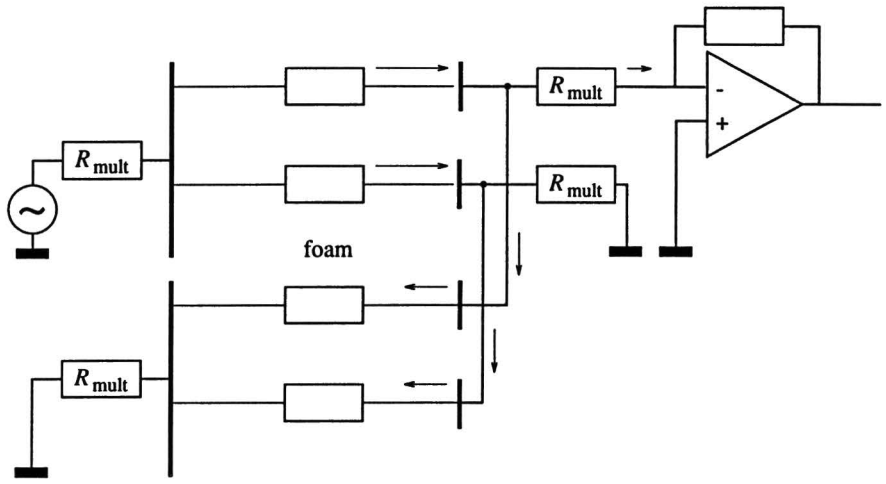

Figure 5.6: *If the resistance of the foam is somewhere below that of the internal resistance of the multiplexer, a significant current can leak away through the foam.*

an idea of these difficulties we will now describe the electronics of the level gauge in some more detail.

The most ideal configuration would be one big plate connected to a source on one side of a foam column and segments all connected to virtual ground by identical opamps. This approach is not practical because it would give a lot of wiring and components. The second problem would be that identical components do not exist and many errors would be introduced this way. The practical solution we made, was using multiplexers. The source plate was cut into smaller plates and only one of them is connected to the source; the remaining plates are connected to earth (see Fig. 5.3). Because all the segments on the opposite side of the tube are connected to zero (real or virtual) this will mean that ideally only the segments opposing the plate connected to the source will experience a current. This makes it possible to interconnect segments opposed to different source plates, because only one segment contributes to the measured current. That reduces the wiring immensely. If we have n segments we could divide the source plate in approximately $\sqrt{n}$ parts opposing $\sqrt{n}$ segments. This reduces the wiring from n wires to $2\sqrt{n}$ wires. We use switches (multiplexers) to connect one of the source plates to the source and the others to ground. Multiplexers are also used to connect one set of interconnected segments to an opamp and the other sets to ground. One configuration of the switches is depicted in Fig. 5.3.

A major source of possible errors were the internal resistance of the multiplexer switches. This can cause segment interaction and other measurement deviations, because segments are not directly connected to earth. Errors will occur when the resistance of the foam is somewhere smaller than that of the switches. If this occurs current will leak away throug the part where $R_{\text{foam}} \ll R_{\text{mult}}$. The current that leaks away is not measured and will cause measurements errors (Fig. ??). These errors are partly corrected for by electronics and partly by the software.

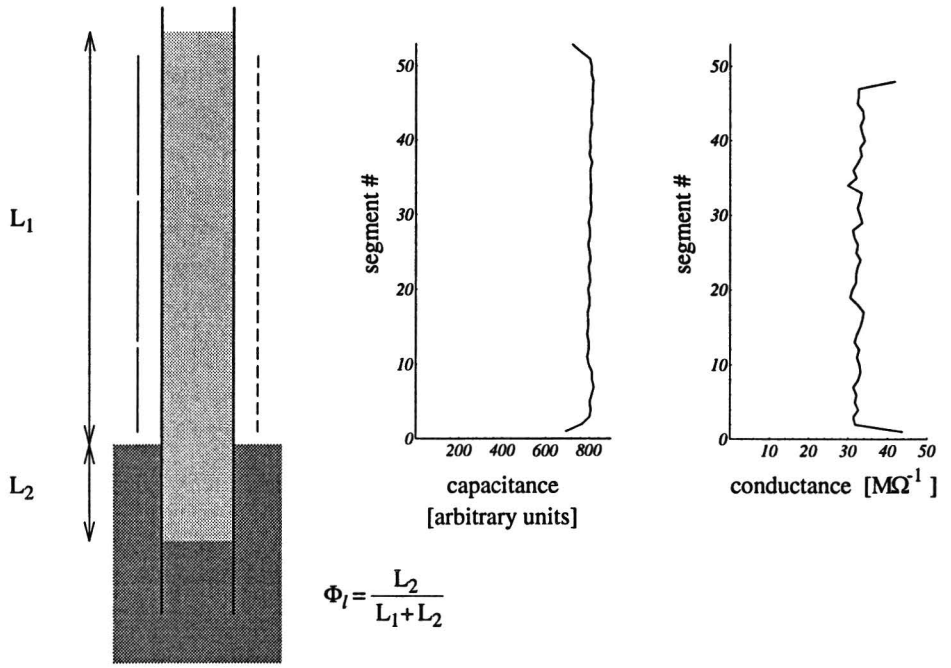

Figure 5.7: *The calibration procedure. Two typical profiles for a uniform wetted foam in the capacitance level gauge and in the resistance level gauge. The boundary effects are typical for the different ways the two gauges are connected to the source.*

5.3 Calibration curves

In chapter 3 (§3.3) we described an effective medium theory which could describe the conductivity and the permittivity in a foam as function of the liquid fraction. To verify the drainage theory, we want to know the liquid fraction. What we measure is capacitance or conductance. To interpret the measurements in terms of liquid fraction calibration measurements were done.

To obtain the calibration data a simple procedure was applied. A tube was filled with a foam of uniform bubble size. This foam was wetted form above at a uniform rate. This created a foam with a uniform liquid fraction. The bottom of the foam rested on the liquid. Using Archimedes law, the part of the foam column under the liquid surface divided by the total height of the column gives the liquid fraction. The level gauge measures an almost constant signal Fig. 5.7. The calibration curve for the conductance level gauge is the easiest to analyse because there are little parasitic effects and it was reproducible. We measured a lot of uniform profiles and we measured the conductance of hundred percent liquid in the level gauge. These two were divided by each other to obtain a relative conductance. Because the geometry for both measurements was the same (namely the level gauge) we expect this relative conductance to be equal to the relative conductivity. The measurements are depicted in Fig. 5.8. Fig. 5.8 combines the calibration data of four different days in one graph. When we took for the pure liquid conductance the value measured on that day, the spread was larger than if we took the mean

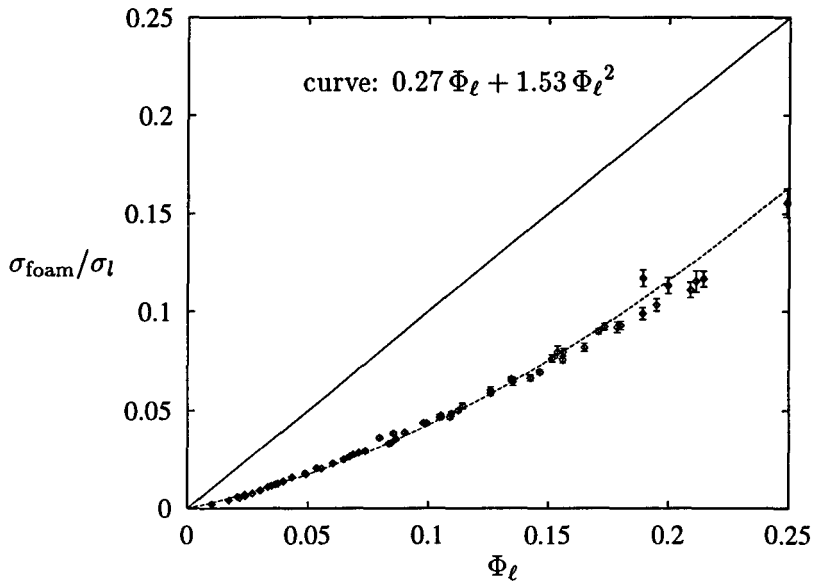

Figure 5.8: *Calibration curve for the conductance level gauge. The depicted curve is a quadratic fit through zero.*

value of the four 100%-measurements. The depicted curve is the graph where we used the mean value of the pure liquid conductance ($550 \pm 25\,\text{M}\Omega^{-1}$). We see that the slope of the curve is smaller than $\frac{1}{3}$.

This calibration curve makes it possible to apply our theory for the effective conductivity of a foam. We will separate the relative liquid fraction in the Plateau borders and in the films. Because the conductivity of the gas can be neglected the formulas reduce to the simplest case. If we rewrite the Eq. (3.22) and Eq. (3.24) with $\sigma_g = 0$ we obtain

$$\begin{aligned} \beta_{\text{eff}} &= \frac{\sigma_{\text{foam}}/\sigma_l}{1-\sigma_{\text{foam}}/\sigma_l}\,\frac{1-\Phi_\ell}{\Phi_\ell} \\ \beta_{\text{eff}} &= \frac{1}{3}\frac{\Phi_{\text{pb}}}{\Phi_\ell} + \frac{2}{3}\frac{\Phi_{\text{film}}}{\Phi_\ell}. \end{aligned} \tag{5.5}$$

The first formula is the Clausius-Mossotti formula and can be used for determining the β_{eff} from the experimental data of Fig. 5.8. We can solve the second formula of Eq. (5.5) and obtain $\Phi_{\text{pb}}/\Phi_\ell$ and $\Phi_{\text{film}}/\Phi_\ell$ (using $\Phi_{\text{pb}} + \Phi_{\text{film}} = \Phi_\ell$). We then obtain Fig. 5.9 Because of the fact that the slope of the measured calibration profile is less then one third, the calculation of Φ_{pb}/Φ_l has the unphysical result that it is larger than one for low liquid fractions (up to 1.5 not shown in the graph). For liquid fractions of about 0.2 the liquid fraction in the films calculated here are to high. This can even be concluded from ordinary optical observation (just looking). The slope of the line however is a bit inaccarate because of the possible error in the measured signal for 100 % liquid.

The calibration curve for the capacitance measurements is depicted in Fig. 5.10.

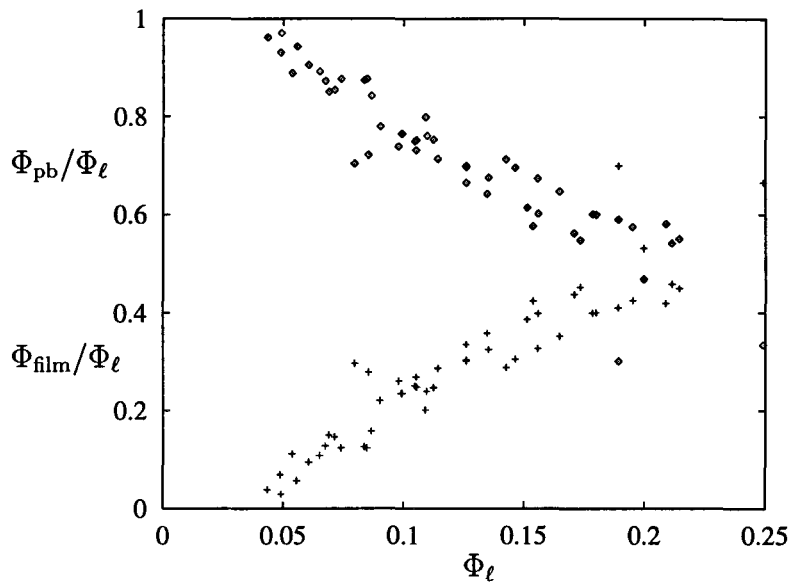

Figure 5.9: *The liquid fraction contained in the Plateau borders and in the films as function of the total liquid fraction* Φ_ℓ.

Only three of the many calibration curves are shown. At zero liquid fraction still a capacitance is measured because of the finite permittivity of the gas phase. We have chosen to show capacitance measurements for different mixtures of water and glycerol. It looks like a saturation point will be reached at a signal of about 2200. This will probably be the point where the parasitic capacitance determines the whole signal. It is shown in the calibration curve that a water ($\varepsilon = 80\varepsilon_0$) glycerine ($\varepsilon = 42\varepsilon_0$) mixture (whose permittivity is lower then that of only water) saturation effects become apparent at much higher liquid fractions. Upon approaching this point the calibration curve is nearly unusable because back translation from signal to liquid fraction will introduce increasingly larger errors. Because it is very difficult to write down the exact form in which parasitic impedances influence the measured signal we did not succeed in obtaining curves only dependent on the characteristics of the foam.

Because of the large effects the conductivity of the liquid has on the measured capacitance, the calibration curves are not easy reproducible. This means that for every set of measurements a new calibration measurement had to be done. This is a great disadvantage compared to the conductance measurements, which gave a reproducible calibration curve.

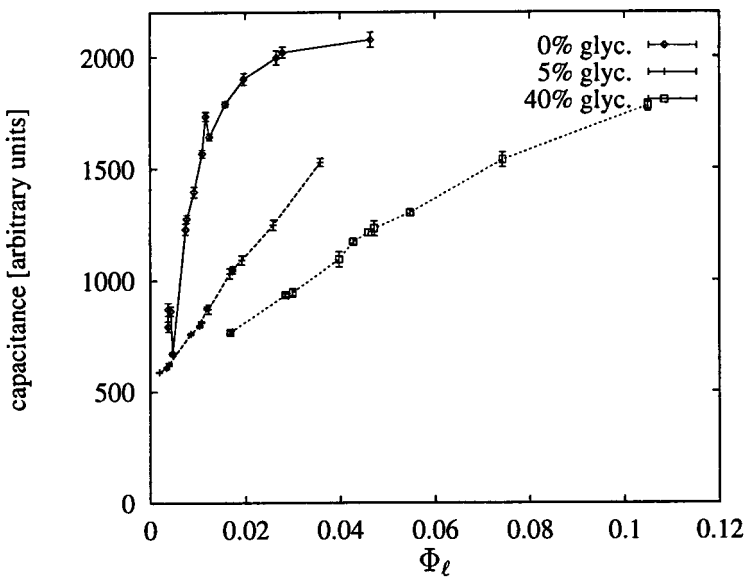

Figure 5.10: *Calibration curves for the capacitance level gauge.*

Chapter 6

Measurements

The measurements can be categorised in different ways. We could have treated the different kind of drainage profiles: the solitary wave, the free drainage curves and pulse waves. The way chosen here is to represent the phenomena which are related to gravitational effects and the phenomena which are related to the pressure term of the drainage equation in different sections. This will give a better understanding of the extent to which the model is validated.

It will be shown that the gravitational effects are proven beyond "reasonable doubt". Effects which have to do with great liquid fraction gradients, and thus a significant pressure term proved to be much more difficult to validate. Making the sectioning in the chosen way will facilitate the discussion. On the other hand it may be difficult for the reader to follow the changes between the profile types, for this we apologise.

The experiments were typical tabletop experiments (see Fig. 5.3). A perspex tube of (2 cm diameter and 70 cm high) was filled with a foam using a narrow capilar to blow the bubbles. The diameter of the bubbles was approximately 3 mm. The liquid used was water with some non-ionic surfactant (0.1%) desolved in it. To vary the viscosity we used glycerine. The forced drainage experiments (solitary waves) were done by submitting water from the top. The flow was started by manually oppening a tab of a buret and to let it then drip, hopefully with constant rate. To measure the free drainage profile we first wetted the foam uniformly in the way descibed above, then turned of the tab and measured the profiles. Pulses were created by turning the tab open and close. Precision to control the amount of water was not needed because we were just interested in asymptotic behaviour.

6.1 Experimental verification

Before we look at the experiments we will first give a summary of the constants required. In the theoretical part of this report we used non-dimensional quantities. Now we need to reintroduce the dimensions so they can be compared to the measurements. This introduction will go in two steps. First we will have to reintroduce time and length by multiplying with the characteristic time and length (Eq. (4.6)). It is then possible to give dimensional expressions for the velocity and

gravitational acceleration	g	9.8	m/ s^2
density	ρ	$1.0\,10^3$	kg/ m^3
surface tension	γ	$73\,10^{-3}$	kg/s^2
viscosity	η	$1.0\,10^{-3}$	kg/m s

Table 6.1: *The needed natural constants.*

constant			value		relations
x_0	=	$\sqrt{\gamma/\rho g}$	$2.73\,10^{-3}$	m	$z = x_0\zeta \;\; R = x_0\sqrt{\alpha}$
t_0	=	$3\eta^*/(C_{area}\sqrt{\rho g\gamma})$	$3.46\,10^{-2}$	s	$t = t_0\tau$
V_0	=	$x_0/t_0 = \gamma C_{area}/3\eta^*$	$7.89\,10^{-2}$	m/s	$V = V_0 v$
$C_{area}x_0t_0$	=	$3\eta^*/\rho g$	$1.52\,10^{-5}$	m s	
p_0	=	$\gamma/x_0 = \sqrt{\gamma\rho g}$	26.8	Pa	$\Delta p = p_0/\sqrt{\alpha}$
$\mathcal{A}_0$	=	$C_{area}x_0^2$	$1.20\,10^{-6}$	m^2	$\mathcal{A} = \mathcal{A}_0\alpha$

Table 6.2: *Important quantities for foam drainage.*

for the Plateau border area. The second step will be to go from Plateau border areas to liquid fractions. To translate the basic measured quantities like conductance and capacitance to liquid fraction is a third step, but this has already been discussed in the previous chapter (§5.3). All the experiments were done with aqueous solutions. In the capacitance measurements we used demi-water with 0.1% surfactant. The surfactant used was Dobanol, a non-ionic surfactant. We did not perform surface tension measurements. Therefore Tab. 6.1 should be considered as listing order-of-magnitudes only.

The next thing we have to do is to translate the liquid fraction Φ_ℓ to the Plateau border area $\mathcal{A}$. Eq. (3.5) gives this relation; the liquid fraction equals the Plateau border area times the Plateau border length l times the number of Plateau borders per unit volume N. If we know the mean bubble volume V_{bubb} it is possible (at least for a monodisperse foam) to calculate the Plateau border length and the number of Plateau borders per unit volume. For a specific structure we have to know the proportionality constant between l and $V_{bubb}^{\frac{1}{3}}$ and we need to know how many Plateau borders can be associated with one bubble. To make a good approximation we will take the bubbles to be Kelvin cells in a periodic cristaline structure. In Fig. 6.1 we depicted a Kelvin cell and how it is constructed. It shows that a Kelvin cell can be constructed from a cube by chipping half of the cube of. We will associate the edges of the Kelvin cell with Plateau borders. One Kelvin cell has 36 edges, each of the same length. Each edge is shared with 3 other cells, so we can associate 12 Plateau borders to one bubble. The volume of a Kelvin cell is half that of the original cube. The edges of the cube are $2\sqrt{2}$ times the length of the edges of the Kelvin cell, so $V_{\text{Kelvin}} = 8\sqrt{2}\,l^3$. We can now conclude

$$N = \frac{12}{V_{bubb}} \tag{6.1}$$

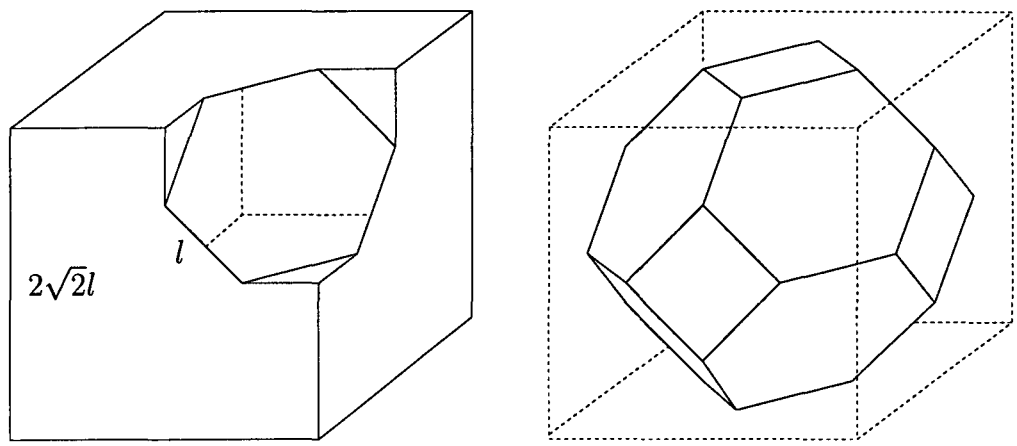

Figure 6.1: *The construction of a kelvin cell.*

$$\begin{aligned} l &= 2^{-\frac{7}{6}} V^{\frac{1}{3}} \\ \Phi_\ell &= 5.35\, V_{bubb}^{-\frac{2}{3}} \mathcal{A}. \end{aligned}$$

So all that is needed is the volume of the bubble which can for example be obtained by counting the number of bubbles that are blown. The bubbles we used had a diameter of approximately 3 mm,

$$\mathcal{A} \approx \Phi_\ell \times 1.1\, 10^{-6} \mathrm{m}^2. \tag{6.2}$$

This is a rough estimation because we did not really determine the bubble diameter accurately. In §4.4 we gave a few constraints which have to be obeyed for the theory to be applicable. We want the characteristic length scale to be larger then the bubble radius to be sure there is a good averaging (Eq. (4.39)). When we compare the x_0 from Tab. 6.1 with the bubble diameter, we see that x_0 is only a few times larger. This means that it is possible there will be phenomena on length scales to small to be handled by this theory. A related criterion was that gradients in the liquid fraction should not be to high Eq. (4.39), curvature of the Plateau borders in their longitudinal direction should be neglegible. For solitary waves this gave the constraint that the non-dimensional velocity is smaller than 1, as seen from Eq. (4.11) this means that its width ($\propto 1/\sqrt{v}$) is greater than one. When using that the non-dimensional velocity of a solitary wave (propagating throug an initial dry foam) is equal to α this gives the constraint

$$\frac{\mathcal{A}}{\mathcal{A}_0} = 0.9\Phi_\ell \ll 1. \tag{6.3}$$

This will certainly be satisfied for small enough liquid fractions. We gave a third criterion. For Plateau borders to govern the drainage the quotient Eq. (4.38) has to be much larger than one. If we believe anything of Fig. 5.9 we are in trouble, because even for $\Phi_\ell = 0.1$ the quotient gives only 1 and for higher liquid fractions it is worse.

6.2 Gravitation induced relations

The gravitational relations are those relations were the (Laplace) pressure term (or the curvature term) can be neglected in comparison to the gravitational term. Roughly speaking we will test relation in which proportionality coefficients appear that do not depend on the surface tension γ. Such an effect is the proportionality of the velocity of a solitary wave propagating through a initial dryed out foam. We saw that this proportionality only dependents on the gravitational term (§4.1). (The pressure term gives the solitary wave front stability and determines its width). If we look at the proportionality constant between the velocity and the liquid fraction we observe that it is independent of the surface tension,

$$\begin{aligned} v &= \alpha \\ \frac{t_0}{x_0} V &= \frac{1}{C_{area} x_0^2} \mathcal{A} \\ V &\approx \frac{V_{bubb}^{\frac{2}{3}}}{5.35 C_{area} x_0 t_0} \Phi_\ell \\ &\approx 0.071 \times \Phi_\ell \frac{\mathrm{m}}{\mathrm{s}} \end{aligned} \tag{6.4}$$

V is the dimensional velocity. Because $x_0 t_0$ is independent of γ so is the proportionality constant.

For free drainage and density pulses propagating through foam we found (§4.3) that there are areas in the tail that are purely determined by the interplay of the gravitational and the viscous forces. In this area of the tail the liquid fraction depends linearly on the position and there was a characteristic time dependency of the slope.

For pulses we gave in the same paragraph the time evolution of the height and the position of the top using the shock wave equation without the pressure term. It is not clear theoretically whether this behaviour will be influenced very much by the pressure term.

The first indication that solitary waves in foam existed was found by Princen [11].He noticed that the velocity of the wavefront was constant in time. Fig. 6.2 is the profile of a solitary wave obtained with the resistance level gauge. The x-axis depicts the segment number, the wave is traveling from left to right. In reality it moves downwards. If we divide the velocity by the liquid fraction we hope to find that is a constant for al solitary wave (moving in a initially dry foam). In this case it is $0.73/0.068 = 10.7$ cm/s which compares favourably with the order-of-magnitude estimation of Eq. (6.4). Therefore the agreement with theory may at least be called good. With the capacitance level gauge we did a whole lot of measurements on solitary waves. Unfortunately we have not had the opportunity to repeat them with the conductance level gauge due to time constrains. The many sets of measurements all needed their own calibration. Fig. 6.2 shows the result of one of these sets. We fitted all the measured waves to a solitary wave profile and determined in this way the velocity and the liquid fraction. In the figure we depicted this velocity as function of the liquid fraction and fitted a straight line. It

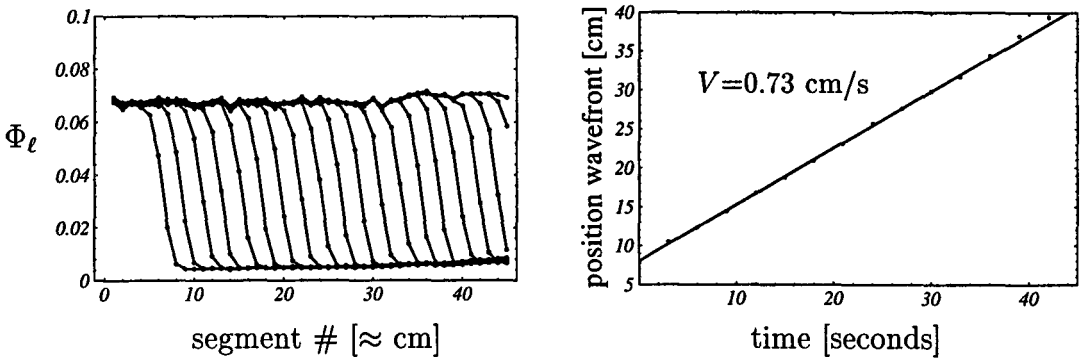

Figure 6.2: *A propagating solitary wave.*

is quite a good fit, although there is much scatter and the line does not go exactly through zero. One of the problems in analysing the data, is that the foam is never completely dry. It is not exactly clear how to deal with the background. Is it in the films and does it not participate in the drainage, or is part of it in the Plateau borders and does it via the sum law have a significant effect on the velocity? The proportionality constant obtained from Fig. 6.3 is 9.4 cm/s. To investigate the gravitational part of the flow we could also look at the sum law directly. Fig. 6.4 shows a beautiful double wave measured with the conductance level gauge. If we analyse it, the wave fronts have a nice linear time dependence and the transition time from the two waves catching up to the final solitary wave is very short. The drawback is that it does not add up, literally. If we sum the velocity of the resulting wave and the initial wave we do not get the velocity of the catch up wave as expected from the theory. The catch-up velocity (0.98 cm/s) is lower than the sum (1.19 cm/s). We first thought it had something to do with the calibration, or with a large background liquid fraction, but it seems impossible to smooth talk it with these arguments. If we look at a small disturbance superimposed on a solitary wave, the velocity of the perturbation should at least be twice that of the underlying wave. Fig. 6.5 shows that this certainly is not the case. These results are very puzzling and we have not really found a plausible satisfying answer for it. Maybe there was some kind of flow at the wall of the tube in the conductance level gauge. Other phenomena that can have participated in a deviation from the theoretical prediction are the flow at the wall of the foam-tube and the diminishing of the number of Plateau borders per unit volume because the foam expands when it is wetted. When taken into account these effects, both of the order Φ_ℓ will diminish the deviation. We were however not capable to explain the whole deviation by considering those effects alone.

When investigating the development of the tails of drainage profiles everything seems to turn out better. Fig. 6.6 shows two free drainage profiles. Note that areas in the tail of these profiles form where the liquid fraction depends linearly on the height. The first of the two shows an initially very moderate wetted foam.

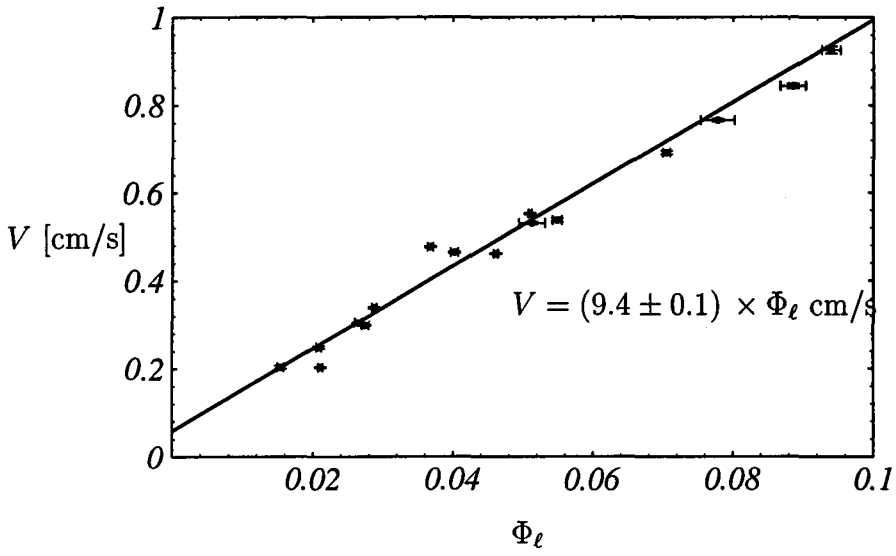

Figure 6.3: *Linearity between liquid fraction and velocity.*

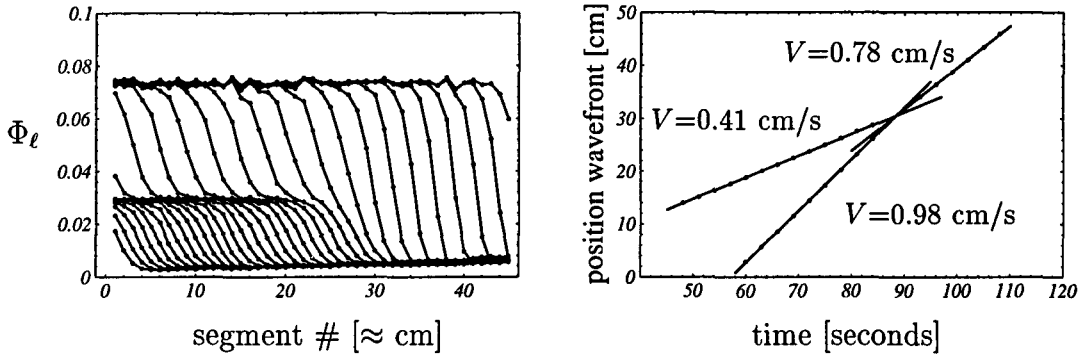

Figure 6.4: *A propagating double wave.*

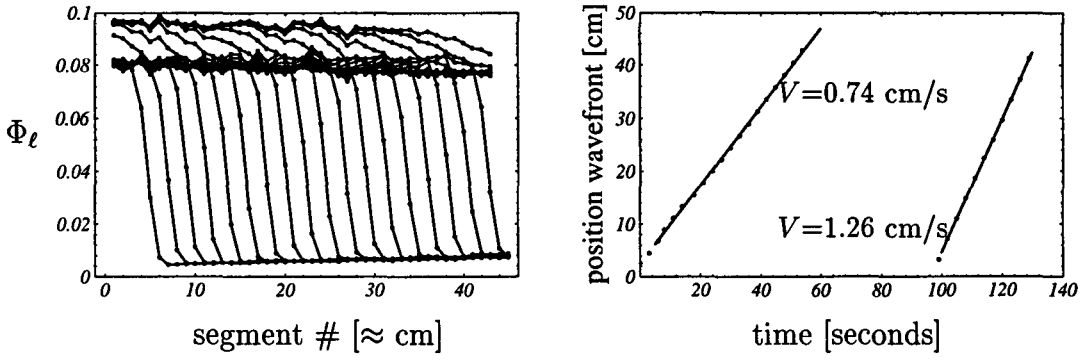

Figure 6.5: *A propagating solitary perturbation wave.*

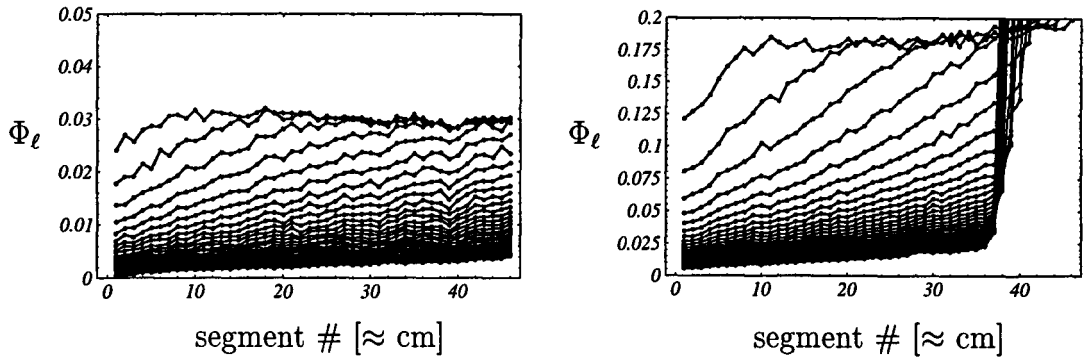

Figure 6.6: *Two free drainage profiles.*

The drainage goes on, until eventually the foam breaks up at the top and the liquid fraction really becomes zero. The drying foam also starts off with the same qualitative behaviour as in the case of drainage without the pressure term, which we neglected in §4.3. The second profile is at a much higher initial liquid fraction. The level is even so high that the liquid level begins to rise significantly when the water drains out of the foam. Near this liquid level we see that the transition layer from foam to liquid is very sharp. This is expected because the characteristic length (This is a pity because it does not make it possible to study the static curve §4.2.2. Secondly it is difficult to determine in this way experimentally what boundary condition must hold just above the transition area.

We will now investigate the second drainage profile in more detail and look at the time dependence of the slope of the tail. Fig. 6.7 depicts in what part in time and in place (between the lines) of the drainage profile we found the theoretically predicted time behaviour. We fitted these indicated parts to lines and have depicted the slope of these lines in the second graph in Fig. 6.7. In §4.3 the time behaviour of the slope in dimensionless units was given by $\frac{1}{2\tau}$ (Eq. (4.32)). Restoring the dimensions we find

$$\text{slope} = \frac{5.35 C_{area} x_0 t_0}{2 V_{bubb}^{\frac{2}{3}}} \frac{1}{t - t_0} \tag{6.5}$$

It is the same constant as in Eq. (6.4) except for a factor two and an inversion. We approximate the slope as being proportional to $(t - t_0)^{-1}$ and fitted t_0 and the proportionality constant. As seen in Fig. 6.7 it is a perfect fit. We found $t_0 = 15.0 \pm 0.5$s and for the constant 0.052 ± 0.007s/cm. If we determine the coresponding constant of Eq. (6.4) we find 9.6 ± 1m/s, which is consistent with the value of 9.4m/s we found for the case of the proportionality of the velocity with the liquid fraction (Fig. 6.3). The third kind of profile which might have properties mainly determined by the gravitational term are pulses. In Fig. 6.8 a pulse is shown. This pulse starts sharp but develops a long tail. Much of the tail behaves like described in §4.3 and the front is sharp enough to try the theoretical

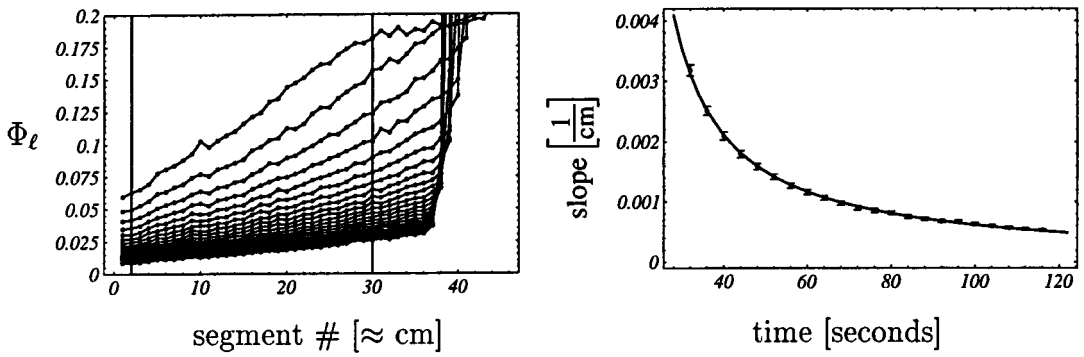

Figure 6.7: *Determining the dependency of the slope of a free drainage profile on the time.*

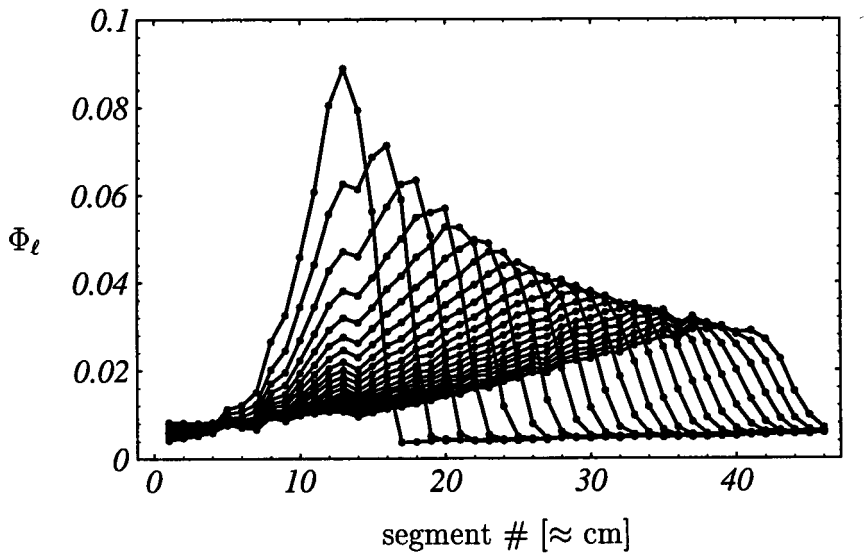

Figure 6.8: *A pulse propagating through a foam.*

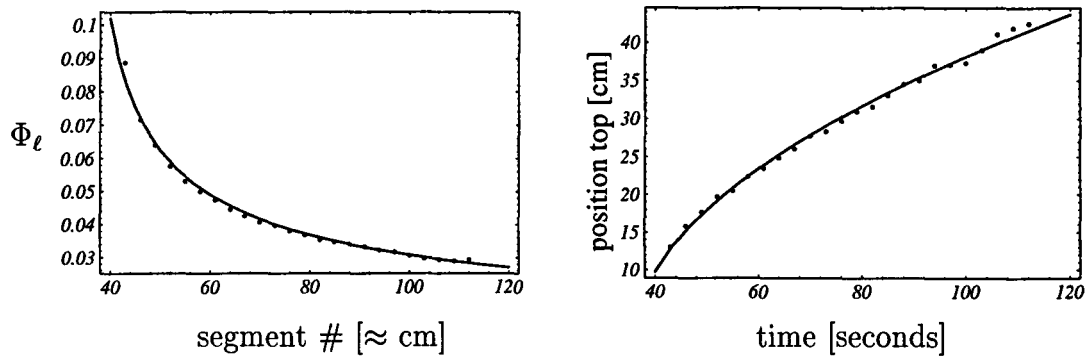

Figure 6.9: *The height and the position of the pulse developing in time.*

profile discussed in §4.3. The top of the pulse has to obey Eq. (4.31). In Fig. 6.9 the time development of the top is given. We expect the height of the height of the top to depend inversely on the square root of the time (minus a t_{start}), and the position is predicted to depend linearly on this square root. The fits are given by

$$(\Phi_\ell)_{top} = \frac{0.25}{\sqrt{t - 35.2}} \tag{6.6}$$
$$z_{top} = 4.76\sqrt{t - 35.8} - 6.4\,\text{cm}$$

Again we can find the proportionality constant of Eq. (6.4). Here it turns out to be $4.76/(2 \times 0.25) = 9.5$cm/s, which (it is starting to get boring is consistent with the earlier found constants. We finally look to the tail of the pulse itself and calculate the slope as function of time. This is done in Fig. 6.10. We see that the time behaviour of this slope is not that good as it was in th case of the free drainage curve. This was expected, Eq. (4.33) and the remarks following it made it clear that it would be harder to find purely gravitational determined areas in the pulse profile. The constant we get in this instance is 0.095 ± 0.006 s/cm which is again consistent with the constants found earlier.

In this section we saw that different phenomena depending only on the gravitational term in of the flow expression, gave consistent results in agreement with the theory. We looked at the propagation velocity of solitary waves, the middle long time behaviour of drainage profiles and the characteristics of density pulses in foam. We also saw some unexplained effect of double waves and perturbations that did not follow the sum law. This is puzzling because the sum law depends only on the gravitational term of the flow term which is otherwise found to determine agree perfectly with the experimental results. Clearly this should be studied further.

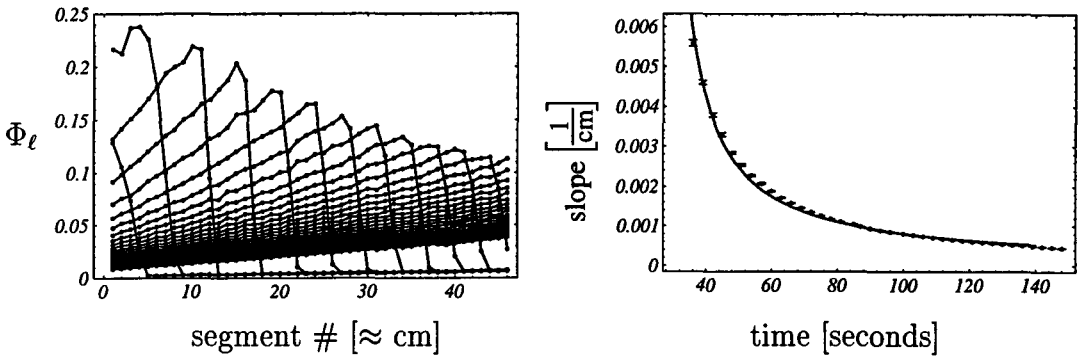

Figure 6.10: *The time evolution of the slope of the tail of a pulse propagating through a foam.*

6.3 Pressure induced relations

To investigate the influence of the Laplace pressure term is more difficult. We only know that it has a stabilising effect and determines the width of profiles in some way. Because x_0 is so small we could not measure static profiles. It would have been the easiest profile to study if we wanted to investigate surface tension related properties of the foam. The broadening of pulses and the influence of Laplace term on the free drainage curves are still not understood theoretically. We have no simple picture how to model them theoretically.

It is obvious that there has to be a stabilising term in the equations, in order that (unphysical) singular shock waves will not occur. It is also clear experimentally that in the last stages of for example free drainage this term will take over. It is however not clear theoretically how. We have done computer simulations but it is unclear what boundary conditions to use.

The form of the pressure term as we describe it determines partly the symmetry properties of the drainage equation. When the symmetry property holds this does not necessarily mean we described the pressure term in the right way, but it is very strong evidence. In practice we only found one way where this symmetry property could be measured quantitatively. It appears in the broadening of the profiles of solitary waves. Our theory predicts that the width (W) of a profile is proportional to the inverse of the square root of its velocity and of that of the liquid fraction. For the relation between the width and the liquid fraction this give theoretically

$$\begin{aligned} w &= \frac{1}{\sqrt{\alpha}} \\ \frac{W}{x_0} &= \sqrt{\frac{5.35\, C_{area} x_0^2}{\Phi_\ell V_{bubb}^{\frac{2}{3}}}} \\ W &\approx 0.010 \times \frac{1}{\sqrt{\Phi_\ell}}\,\text{m}. \end{aligned} \tag{6.7}$$

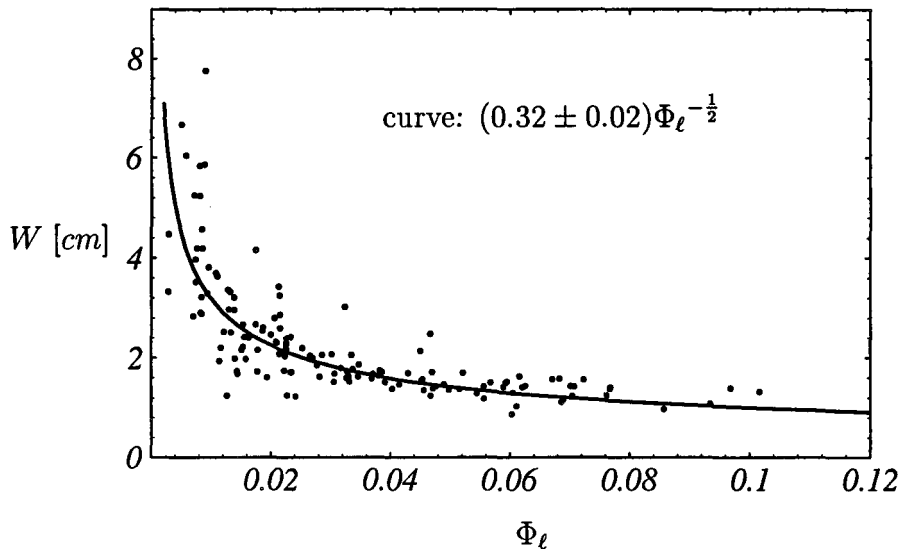

Figure 6.11: *Width of the solitary waves as function their liquid fraction.*

We have not yet determined this width with the resistance level gauge, but have done extensive measurements with the capacitance level gauge. Making quantitative statements about the broadening proved to be very difficult because of great scatter in the data. This problem was related to the difficulties with the calibration curves, and with the extra broadening caused by the inhomogeneous field. We tried to compensate for the broadening. Even then, it was only possible to make a very rough graph of the many points Fig. 6.11, see the great scatter in the data points. We look at the relation between the width of the solitary wave and the liquid fraction because this relation is independent of the viscosity. In Eq. (6.7) we see no dependency on t_0, only on x_0 which is independent of η^*. This makes it possible to use data measured for different viscosities for the same fit.

When fitting the data to $1/\sqrt{\Phi_\ell}$ we find a proportionality constant of (0.32 ± 0.02) cm/s this is three times smaller than the theoretical predicted one. Because of the uncertainty in the bubble size and in the surface tension, this is as good a value as we can expect.

We have a second theoretical prediction involving the pressure term which can be compared to measurement. This is the predicted time behaviour of the tail of a free drainage (and of the pulse) profile. This had to do with the no-flow boundary condition that had to be satisfied at the top of the foam Eq. (4.36). This is being looked into at the moment, we have not yet definite results.

6.4 Effective viscosity

The flow term predicted by the theory assumes Poiseuille flow through the Plateau borders, for which we introduced an effective viscosity. The close agreement of the gravitational flow term with the experiments give a good indication that this

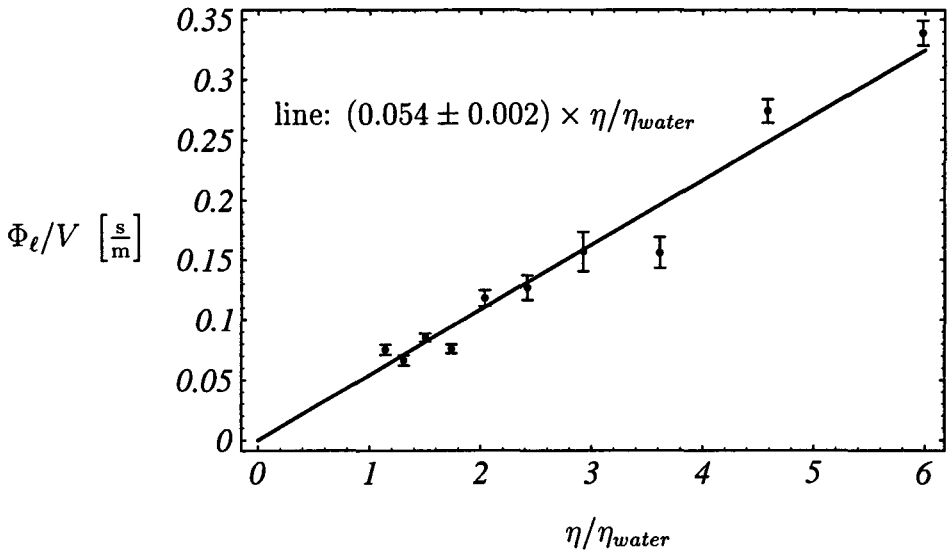

Figure 6.12: *Linear dependence between Φ_ℓ/V and η.*

assumption is right. The predicted theoretical values and the experimentally found ones are not too far off. Therefore we might have some confidence in calculating the effective viscosity dependence on the shape of the Plateau border.

An additional test is to see if the linearity between the effective viscosity and liquid viscosity holds. By adding glycerine to the water surfactant solution we increased the viscosity. At a certain viscosity we measured many solitary wave profiles and determined the proportionality constant between the velocity and liquid fraction. The inverse of this constant depends linearly on the effective viscosity. In Fig. 6.12 we plotted the constant against the liquid viscosity. Unfortunately these measurements were done with the capacitance level gauge too, so again great scatter in the data points is seen. The points do not form a very convincing line, but they do not form any other curve convincingly either. This means that more precise measurements and more data points are needed. The constant we hope to have measured as function of the the viscosity is

$$\frac{5.35C_{area}x_0t_0}{V_{bubb}^{\frac{2}{3}}} = \left(\frac{5.35C_{area}x_0t_0}{V_{bubb}^{\frac{2}{3}}}\right)_{\text{water}} \times \frac{\eta^*}{\eta^*_{\text{water}}} = \left(\frac{5.35C_{area}x_0t_0}{V_{bubb}^{\frac{2}{3}}}\right)_{\text{water}} \times \frac{\eta}{\eta_{\text{water}}}$$

We calculated this constant for water now a few times already. When we calculate the slope of the fitted line we should obtain that constant again. The slope is (0.054 ± 0.002) s/m. The constants we found for the other measurements (the solitary wave, the free drainage profile) all gave a value of 0.1s/m. The measured constant is a factor two of compared with the others.

Chapter 7

conclusions

In this thesis a drainage model (based on [15]) is derived and fully motivated. For low liquid fractions the drainage is governed by Plateau borders. The network structure of Plateau borders is taken into account.

The resulting partial differential equation is a non-linear equation for the cross-sectional area of the Plateau borders and proved to be generic. Two characteristic dimensions are needed: a characteristic time and a characteristic length scale.

Some analytic results were found. The most interesting of these was the solitary wave solution. Besides the exact solutions we found good approximations for free drainage profiles and pulses propagating through foam.

The averaging needed to take into account the Plateau border structure was general. It provided a technique not only to describe drainage but also conductivity. A still more general, preliminary effective medium theory was developed to describe the capacitance of a foam and including the interesting analogy for the thermal conductance.

The drainage was studied experimentally. We use two apparatuses. One was based on segmented capacitance measurement the other on conductance measurement. These *level gauges* enabled position dependent monitoring of the liquid fraction in a foam column. Evolving drainage profiles were studied. To obtain the liquid fraction we had to do calibration measurements. These measurements were to some extent explained using the effective material expressions we derived. Having the calibration curves, we performed quantitative measurements to verify the drainage model.

The level gauges proved to be very suitable for measuring drainage profiles. The conductance gauge, especially designed for this foam research gave excellent results. Measurements done with the capacitance level gauge are more difficult to interpret due to uncertainties in the calibration.

We did three kind of measurements on foam drainage. Solitary waves were studied using the capacitance level gauge. We obtained the (by the theory predicted) proportionality of their velocity and the liquid fraction. The found proportionality constant agreed with the theory. We tried to measure the width of the profiles but this proved to be much more difficult. The same kind of difficulties arose when

trying to determine the relationship between the effective viscosity and the liquid viscosity.

The conductance level gauge was mainly used to measure free drainage profiles and pulses. The results were all consistent with each other and with a rough theoretical estimate. The measurement of double waves gave some puzzling results. A first attempt was made to use the effective medium theory for fitting the calibrations.

The measurements show a good agreement of theory and experiment, although the propagation of double waves in foam should be submitted to further investigations. The influence of the Laplace pressure term of the equation deserves further study. The width of the solitary waves contain information about this term. Therefore the width measurements should be repeated with the conductance level gauge.

Although the effective medium theory developed for foam is just preliminary, it introduced some new averaging of important structures. These can be used to describe thermal conductance of foams of obvious importance for polyurethane processing.

Appendix A

Derivation of the Laplace-Young equation

Minimasation of the free energy(F) gives

$$\delta F = \gamma\,\delta A - \Delta p\,\delta V = 0, \tag{A.1}$$

with:

$$\delta V = \int\int \mathbf{w}\cdot\delta\mathbf{x}\,d\mu_1 d\mu_2, \tag{A.2}$$

$$A = \int\int |\mathbf{w}|\,d\mu_1 d\mu_2,$$

$$\delta A = \int\int \frac{\partial|\mathbf{w}|}{\partial x_{j,\mu_i}}\,\delta x_j\,d\mu_1 d\mu_2,$$

$$= -\int\int \partial_{\mu_i}\left(\frac{\partial|\mathbf{w}|}{\partial x_{j,\mu_i}}\right)\delta x_j\,d\mu_1 d\mu_2,$$

and

$$\mathbf{w} = \mathbf{x}_{,\mu_1}\times\mathbf{x}_{,\mu_2}.$$

This results in

$$\gamma\,\partial_{\mu_i}\frac{\partial|\mathbf{w}|}{\partial x_{j,\mu_i}} + \Delta p\,w_j = 0. \tag{A.3}$$

Locally we can always take a parametrisation that gives

$$\mathbf{x}_{,\mu_i}\cdot\mathbf{x}_{,\mu_j} = \delta_{ij} \quad \Rightarrow |\mathbf{w}| = 1, \tag{A.4}$$

$$\delta(\mathbf{x}_{,\mu_i}\cdot\mathbf{x}_{,\mu_j}) = 0 \quad \text{to the first order,}$$

so

$$\mathbf{x}_{,\mu_i\mu_j}\cdot\mathbf{x}_{,\mu_k} = 0 \quad \forall\, i,j,k. \tag{A.5}$$

Here

$$\frac{\partial|\mathbf{w}|}{\partial x_{j,\mu_i}} = \frac{1}{|\mathbf{w}|}\frac{\partial\mathbf{w}^2}{\partial x_{j,\mu_i}} = \frac{\partial\mathbf{w}^2}{\partial x_{j,\mu_i}} = x_{j,\mu_i}, \tag{A.6}$$

$$\partial_{\mu_i}\frac{\partial|\mathbf{w}|}{\partial x_{j,\mu_i}} = \frac{\partial^2}{\partial\mu_i\partial\mu_i}x_j. \tag{A.7}$$

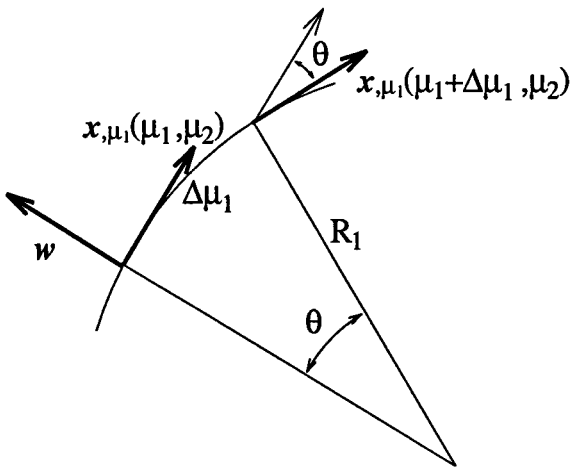

Figure A.1: principal radius of curvature R_1

Thus locally in this parametrisation :

$$\frac{\partial^2}{\partial\mu_i\partial\mu_i}\mathbf{x} = -\frac{\Delta p}{\gamma}\mathbf{w} \tag{A.8}$$

According to Eq. (A.5) both $\partial^2_{\mu_1}\mathbf{x}$ and $\partial^2_{\mu_2}\mathbf{x}$ are parallel with $\mathbf{w}$. Eq. (A.8) can be interpreted by introducing principal radii of curvature as illustrated in Fig. A.1. Take μ_2 =constant and note the following elementary relations

$$\begin{aligned} \mathbf{x}_{,\mu_1}(\mu_1+\Delta\mu_1)\cdot\mathbf{x}_{,\mu_1}(\mu_1) &= |\mathbf{x}_{,\mu_1}(\mu_1+\Delta\mu_1)|\,|\mathbf{x}_{,\mu_1}(\mu_1)|\cos\theta, \\ \theta &= \frac{\Delta\mu_1}{R_1}+O(\Delta\mu_1^2) \end{aligned} \tag{A.9}$$

Making a Taylor expansion of $\mathbf{x}_{\mu_1}$ and using Eq. (A.5) one gets

$$\begin{aligned} \mathbf{x}_{,\mu_1}(\mu_1+\Delta\mu_1) &= \mathbf{x}_{,\mu_1}(\mu_1)+\mathbf{x}_{,\mu_1\mu_1}\,\Delta\mu_1+\frac{1}{2}\partial^3_{\mu_1}\mathbf{x}\,\Delta\mu_1^2+O(\Delta\mu_1^3) \\ ,\mathbf{x}_{,\mu_1}(\mu_1+\Delta\mu_1)\cdot\mathbf{x}_{,\mu_1}(\mu_1) &= 1+\frac{1}{2}\mathbf{x}_{,\mu_1}\cdot\partial^3_{\mu_1}\mathbf{x}\,\Delta\mu_1^2+O(\Delta\mu_1^3) \\ ,|\mathbf{x}_{,\mu_1}(\mu_1+\Delta\mu_1)| &= 1+\frac{1}{2}\left(\mathbf{x}^2_{,\mu_1\mu_1}+\mathbf{x}_{,\mu_1}\cdot\partial^3_{\mu_1}\mathbf{x}\right)\Delta\mu_1^2+O(\Delta\mu_1^3). \end{aligned} \tag{A.10}$$

When expanding the cosine too, Eq. (A.9) gives

$$\begin{aligned} &1+\frac{1}{2}\mathbf{x}_{,\mu_1}\cdot\partial^3_{\mu_1}\mathbf{x}\,\Delta\mu_1^2 = \\ &\left(1+\frac{1}{2}\left[\mathbf{x}^2_{,\mu_1\mu_1}+\mathbf{x}_{,\mu_1}\cdot\partial^3_{\mu_1}\mathbf{x}\right]\Delta\mu_1^2\right)\left(1-\frac{1}{2}\frac{\Delta\mu_1^2}{R_1^2}\right)+O(\Delta\mu_1^3), \end{aligned} \tag{A.11}$$

thus

$$\frac{1}{R_1} = |\mathbf{x}_{,\mu_1\mu_1}|, \tag{A.12}$$

and because the choise of R_1 as in Fig. A.1 $\mathbf{x}^2_{,\mu_1\mu_1}$ is opposite to $\mathbf{w}$ when R_1 is positive. Combining Eq. (A.8) and Eq. (A.12) gives the Laplace-Young equation

$$\frac{1}{R_1}+\frac{1}{R_2} = \frac{\Delta p}{\gamma}. \tag{A.13}$$

Appendix B

Isotropic averaging of a symmetric matrix

In effective material calculations it is sometimes needed to average over all orientations. This calculation will now be done for a symmetric matrix ($\mathbf{M} : R^n \rightarrow R^n$). It will be notated as

$$\langle \mathbf{M} \rangle = \frac{\int \mathcal{D}\mathbf{O}\, \mathbf{O}\, \mathbf{M}\, \mathbf{O}^{\mathbf{T}}}{\int \mathcal{D}\mathbf{O}}, \tag{B.1}$$

$\mathbf{O}$ are orthogonal matrices with determinants 1 (elements of the rotation group SOn), and the integration is done with the right weight for that group.

A symmetric matrix is always diagonalisable with real diagonal elements and can be written as

$$\mathbf{M} = \tilde{\mathbf{O}} \mathbf{\Lambda} \tilde{\mathbf{O}}^{\mathbf{T}}, \tag{B.2}$$

where $\tilde{\mathbf{O}}$ is some orthogonal matrix and $\mathbf{\Lambda}$ a real valued orthogonal matrix with element that correspond to the eigenvalues of $\mathbf{M}$. Because $\tilde{\mathbf{O}}$ is orthogonal

$$\langle \mathbf{M} \rangle = \frac{\int \mathcal{D}\mathbf{O}\, \mathbf{O}\, \mathbf{\Lambda}\, \mathbf{O}^{\mathbf{T}}}{\int \mathcal{D}\mathbf{O}}. \tag{B.3}$$

The elements of $\mathbf{\Lambda}$ can be permuted by the use of an matrix of SOn, e.g.

$$\begin{pmatrix} 0 & 1 & & \\ -1 & 0 & & \\ & & 1 & \\ & & & \ddots \end{pmatrix} \begin{pmatrix} \lambda_1 & & & \\ & \lambda_2 & & \\ & & \lambda_3 & \\ & & & \ddots \end{pmatrix} \begin{pmatrix} 0 & -1 & & \\ 1 & 0 & & \\ & & 1 & \\ & & & \ddots \end{pmatrix} = \begin{pmatrix} \lambda_2 & & & \\ & \lambda_1 & & \\ & & \lambda_3 & \\ & & & \ddots \end{pmatrix}$$

Thus if the elements of $\mathbf{\Lambda}$ are permuted we still get the same average. Because $\langle \mathbf{I} \rangle = \mathbf{I}$, this gives for the summation over all $(n!)$ permutations of the diagonal matrix $\mathbf{\Lambda}$

$$\langle \mathbf{M} \rangle = \frac{1}{n!} \left\langle \sum_{\text{perm}} \mathbf{\Lambda} \right\rangle = \frac{(n-1)!}{n!} \sum_i \lambda_i \langle \mathbf{I} \rangle = \frac{1}{n} \mathrm{Tr}(\mathbf{\Lambda})\, \mathbf{I} = \frac{1}{n} \mathrm{Tr}(\mathbf{M})\, \mathbf{I} \tag{B.4}$$

Bibliography

[1] G.K. BATCHELOR, *An Introduction to Fluid Dynamics*, 179-181.

[2] J.J. BIKERMAN, *Foams*, Springer-Verlag, Berlin (1973).

[3] N.O. CLARK, *The electrical conductivity of foam*, Trans. Faraday Soc. **44**, 13-15 (1948).

[4] A.K.DATYE, R. LEMLICH, *Liquid distribution and electrical conductivity in foam*, Int. J. Multiphase Flow **9**, 627-636 (1983).

[5] I.I. Goldfarb, K.B. Kann and I.R. Schreiber, *Liquid flow in foams*, Izvestiya Akademii Nauk SSSR **2**, 103-108 (1987).

[6] A.M. KRAYNIK, *Foam drainage*, Sandia Report, SAND83-0844.

[7] L. KRUGLYAKOV, L.L. KUZNETSOVA, KH. I. KRISTOV AND D.R. EKSEROVA, *synergetics of foams with high pressure drops in Plateau-Gibbs channels*, Kolloidnyi Zhurnal **41**, 445-452 (1979).

[8] R. LEMLICH, *A theory for the limiting conductivity of polyhedral foam at low density*, J.Col.Interface Sci. **46**,107-110 (1978).

[9] R. A. LEONARD AND R. LEMLICH, *A study of interstatial liquid flow in foam*, A.I.Ch.J. **11**, 18-29 (1965).

[10] K.J. MYSELS, K. SHINODA & S. FRANKEL, *Soap films, studies of their thinning and a bibliography*, Pergamon Press, Oxford (1959).

[11] H.M. PRINCEN, *J. Coll Interf. Science* **134**, 188 (1990).

[12] F. SHIH AND R. LEMLICH, *A study of interstatial liquid flow in foam*, A.I.Ch.J. **13**, 751-754 (1967).

[13] F. SHIH AND R. LEMLICH, *Continuous foam drainage and overflow*, Ind.Eng.Chem. **10**, 254-260 (1971).

[14] J. VAN DER STEEN, unpublished (1985).

[15] G. VERBIST AND D. WEAIRE, *Europhys. Lett*, **26** (8), (1994) 631.

[16] G. VERBIST AND D. WEAIRE, 1994 (to be published).

[17] G. VERBIST, D. WEAIRE & J. EARNSHAW, (to be published).

[18] D. WEAIRE, N. PITTET, S. HUTZLER & D. PARDAL, *Steady state drainage of an aqueous foam*, Phys. Rev. Lett. **71**, 2670 (1993).

[19] E.ZAUDERER, *Partial Differential Equations of Applied Mathematics.*